

MATHEMATICS OF MICROORGANISM SWIMMING IN MICROPOLAR FLUIDS

A Thesis

by

SHANKAR NARASIMHA

BS, Visvesvaraya Technological University, 2016

Submitted in Partial Fulfillment of the Requirements for the Degree of

MASTER OF SCIENCE

in

MATHEMATICS

Texas A&M University-Corpus Christi
Corpus Christi, Texas

December 2021

©Shankar Narasimha

All Rights Reserved

December 2021

MATHEMATICS OF MICROORGANISM SWIMMING IN MICROPOLAR FLUIDS

A Thesis

by

SHANKAR NARASIMHA

This thesis meets the standards for scope and quality of
Texas A&M University-Corpus Christi and is hereby approved.

D. Palaniappan, PhD
Chair

Lea-Der Chen, PhD
Committee Member

S. M. Mallikarjunaiah, PhD
Committee Member

December 2021

ABSTRACT

Typical representation of the swimming motion of microorganisms in fluid environments model the microorganisms as spherical squirmers in a viscous fluid (Newtonian Fluid) with prescribed surface velocities on the squirmer surface. There are numerous fluids in nature that deviate from the classical Newtonian fluid, such as human and animal blood. Modeling swimming mechanisms in these non-classical fluid settings can be very useful but are mathematically challenging. In this thesis, we develop and analyze a mathematical model for the swimming of microorganisms in micropolar fluids - the fluids that depart from the classical Newtonian fluid due to the micro-rotational effect. Specifically, micropolar fluid continuum equations involve both the velocity and internal spin vector fields resulting in antisymmetric and couple stresses. The mathematical problem of swimming in micropolar fluids is analyzed via a spherical squirmer model in the absence of inertial effects and assuming steady motion. The idealized configuration allows exact analytical solutions for the velocity and spin fields surrounding the squirmer via Stokes's stream function formulation. Effects of normal and tangential modes induced on the surface of the squirmer are explained for the two-Mode squirmer. Closed-form expressions for the physical quantities involving the n -Mode general case are also reported. Our exact solutions to the boundary value problem (BVP) for the sixth-order partial differential equation (PDE) contain previously derived results for Stokes and Brinkman fluid squirmer models. It is observed that the propulsion speed, calculated using the force-free condition, depends on the first surface velocity mode only. Surprisingly, the swimming speed in a micropolar fluid is the same as that of the spherical microorganism swimming velocity in Newtonian (Stokes) fluids. The power dissipation and swimming efficiency results derived using non-zero spin boundary conditions on the squirmer surface, however, reveal the micro-rotational effects due to the inclusion of higher surface velocity modes. The two-mode analytical results are further utilized to inspect the structure of flow fields surrounding the spherical. Our exact mathematical results presented herein may be of interest in understanding microorganisms swimming mechanisms in fluids that exhibit angular momentum due to internal micro-rotation.

ACKNOWLEDGEMENTS

First and foremost, I would like to express my sincere thanks to, Dr. D. Palaniappan, thesis committee chair. The door to his office was always open whenever I ran into trouble or had a question or doubt about the research or writing. He consistently allowed this thesis to be my work but steered me in the right direction whenever he thought I needed it. His immense knowledge, vast experience, and expertise have encouraged me all the time. He was very patient with knowledge gaps in the area. Without his assistance and dedicated involvement in every step throughout the process, the thesis would never have been accomplished.

I express my profound gratitude to Dr. Lea-Der Chen and Dr. S. M. Mallikarjunaiah, thesis committee members, for their technical support on my study, invaluable advice, continuous support, and patience during my master's study. Most importantly, none of this could have happened without their guidance.

I would like to thank Dr. S. M. Mallikarjunaiah, for his support and guidance that put me in the right direction to pursue my career in the field of my interest. I wish to express my sincere thanks to Dr. Alexey Sadovski for providing me with the required knowledge and opportunity not only for the completion of my master's program but also for a better understanding of mathematics.

I would like to thank the Office of PROVOST for funding to present the research results at *American Physical Society-Division of Fluid Dynamics* held during November 22nd - 24th, 2020. Also, I would like to thank Dr. S. B. Sathyanarayana, a mathematics professor in India for his encouragement and guidance to pursue my career in the field of mathematics.

I would like to thank my closest friends Pavithra, Karthik, Abhilash, Pratiksha, and Sharath for their understanding, and moral support that helped me in this journey.

Finally, I would like to thank my parents for their blessings and guidance that provided me strength to overcome difficult situations. It would have been impossible for me to finish my studies without their tremendous understanding and constant support.

DEDICATION

To my parents and mentors.

TABLE OF CONTENTS

	Page
ABSTRACT	iv
ACKNOWLEDGEMENTS	v
DEDICATION	vi
TABLE OF CONTENTS	vii
LIST OF FIGURES	ix
LIST OF TABLES	xi
NOMENCLATURE	xii
CHAPTER I: INTRODUCTION	1
CHAPTER II: MATHEMATICAL FORMULATION	6
2.1 Basic Equations	6
2.2 Axisymmetric Flow in Spherical Polar Coordinates	7
2.3 Boundary Conditions for Spherical Squirmer	10
2.4 Derivation of the General Solutions	11
CHAPTER III: TWO-MODE AND n -MODE ANALYTICAL SOLUTIONS FOR A SPHERICAL SQUIRMER	18
3.1 Two-Mode Results for the Stream function, Velocity, Micro-rotation and Stress Components	19
3.2 Swimming Speed, Power and Efficiency Calculations from the 2-Mode Solutions	25
3.3 n -Mode Results for a Squirmer in Micropolar Fluid	28
CHAPTER IV: INTERPRETATIONS OF TWO-MODE RESULTS FOR A SPHERICAL SQUIRMER IN MICROPOLAR FLUID	33
4.1 Features of 1-Mode Results	33
4.2 Power and Efficiency for Two-Mode Results	34
4.3 Stokes Flow Dominance and Some Streamline Patterns	38
4.4 Flow structure for Two-Mode Spherical Squirmer in Micropolar Fluids	41

CHAPTER V: SUMMARY AND CONCLUSION	44
APPENDIX A: Recurrence Relation for the Modified Spherical Bessel Functions of the Third Kind	46
APPENDIX B: Certain Properties of the Associated Legendre Functions	47
REFERENCES	48

LIST OF FIGURES

	Page	
1.1	Reproduced from reference [14]: Microscopic swimmers (a) <i>E. Coli</i> , (b) <i>C. crescentus</i> . (c) <i>R. sphaeroides</i> (d) <i>Spiroplasma</i> (e) <i>Human spermatozoa</i> (f) <i>Mouse spermatozoa</i> (g) <i>Chlamydomonas</i> . (h) <i>Paramecium</i>	1
1.2	Reproduced from reference [20]: (a) A scanning electron micrograph of <i>Paramecium caudatum</i> (150 μ m long) depiction of form and orientation of cilia beating on a forward-swimming cell. (b) Detail of a region of a similar micrograph from another cell showing a prominent recovery wave R and a less obvious band of cilia in their power stroke P.	2
1.3	Reproduced from reference [2]: Surface oscillation/velocity represented due to the cilia beating	3
2.4	Spherical Polar Coordinates System	8
2.5	Representation of spherical microorganism placed in a micropolar fluid	10
4.6	Variation of power vs α for (a) $A_2 = A_1 = 1$ and $B_1 = B_2 = 0$, (b) $A_2 = A_1 = 0$ and $B_1 = B_2 = 1$, (c) $A_2 = A_1 = 1$ and $B_1 = 1, B_2 = 2$	35
4.7	Variation of power vs ε for (a) $A_2 = A_1 = 1$ and $B_1 = B_2 = 0$ (b) $A_2 = A_1 = 0$ and $B_1 = B_2 = 1$ (c) $A_2 = A_1 = 1$ and $B_1 = 1, B_2 = 2$	36
4.8	Variation of efficiency vs α for (a) $A_1 = A_2 = 1$ and $B_1 = B_2 = 0$ (b) $B_1 = B_2 = 1$ and $A_1 = A_2 = 0$ (c) $B_1 = 1, B_2 = 2$ and $A_1 = A_2 = 1$	37
4.9	Variation of efficiency vs ε for (a) $A_1 = A_2 = 1$ and $B_1 = B_2 = 0$ (b) $B_1 = B_2 = 1$ and $A_1 = A_2 = 0$, (c) $B_1 = 1 B_2 = 2$ and $A_1 = A_2 = 1$	38
4.10	Streamline plots for $\alpha = 0.5, \nu = 2.9 \times 10^{-4}, \nu_r = 2.32 \times 10^{-3}, \gamma = 10^{-6}$ (a) Stokes Flow (b) Brinkman Flow (c) Micropolar Flow	41
4.11	Swimming motion of the squirmer $\alpha = 0.5, \nu = 2.9 \times 10^{-4}, \nu_r = 2.32 \times 10^{-3}, \gamma = 10^{-6}$ (a) Pusher (b) Neutral (c) Puller	42

4.12 Micro-rotation distribution around the surface of the squirmer for $\alpha = 0.5$, $\nu = 2.9 \times 10^{-4}$, $\gamma = 10^{-6}$ (a) $v_r = 2.32 \times 10^0$ (b) $v_r = 2.32 \times 10^{-5}$ (c) $v_r = 2.32 \times 10^{-10}$. . 43

LIST OF TABLES

	Page
4.1 Stream function values for closer x -coordinate values of a point in the fluid domain . .	40
4.2 Stream function values for farther x -coordinate values of a point in the fluid domain . .	40

NOMENCLATURE

μ, k, λ_1	Material Constants
ν	Classical Newtonian Viscosity
ν_r	Rotational Viscosity
$\alpha_1, \beta_1, \gamma$	Angular Viscosity Coefficients
r, θ, ϕ	Spherical Polar Coordinates
\mathbf{u}, Ω	Velocity and Micro-rotational Vector, respectively
α	Non-zero Micro-rotation
u_r^{2M}, u_θ^{2M}	Radial and Tangential Components of velocity vector for 2-mode respectively
Ω^{2M}	ϕ -Component of the Micro-Rotation vector for 2-mode squirmer
A_n, B_n	Radial and Tangential modes of Oscillations
ψ	Stream Function
$I_{n+\frac{1}{2}}, K_{n+\frac{1}{2}}$	Modified Spherical Bessel Functions of the First and Third kinds for $n \in \mathbb{Z}$
p	Pressure
$T_{rr}^{2M}, T_{r\theta}^{2M}$	Radial and Tangential Components of Stress tensor for 2-mode squirmer
F_r	Drag Force
U	Swimming Speed/Velocity
P^{2M}	Power for 2-mode squirmer
η	Hydrodynamic Efficiency
u_r^{nM}, u_θ^{nM}	Radial and Tangential Components of velocity vector for n-mode respectively
Ω^{nM}	ϕ -Component of the Micro-Rotation vector for n-mode squirmer respectively
$T_{rr}^{nM}, T_{r\theta}^{nM}$	Radial and Tangential Components of Stress tensor for n-mode squirmer
P^{nM}	Power for n-mode squirmer

CHAPTER I: INTRODUCTION

¹ Swimming microorganisms are found inside people such as gut bacteria, sperm, and outside for instance algae and bacteria in bio-reactors, lakes, and ocean. Typically, microorganisms covered with flagella or cilia (see Figure 1.1), propel themselves in a fluid by beating these appendages in coordinated fashions [5, 10, 21, 22]. Such a self-propulsion at small length scales (in nanometers, nm) is widely observed in biological processes including spermatozoa reaching the ovum during reproduction, microorganisms escaping predators, and microbes hunting for food [3, 9]. As narrated in Brennen and Winet [4] cilia or flagella are a group of contractile elements that oscillate to propel the microorganism in fluid environments. Water propulsion by cilia attached to a single-celled microorganism (Figure 1.2) has been discussed in [20]. Many theoretical models describing the propulsion mechanisms of microorganisms in Newtonian fluids have been proposed (see [4, 22], for instance). It is evident from the proposed models that the determination of swimming characteristics relies on the solutions of the mathematical boundary value problem for the governing partial differential equations. In this, we provide a mathematical model and calculations for a swimming spherical body resembling a microorganism in micropolar fluids.

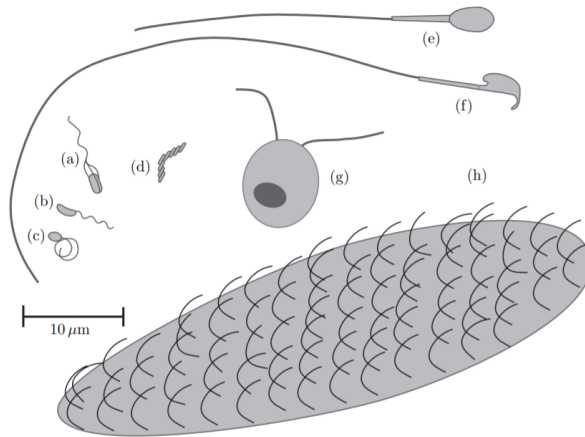


Figure 1.1

Reproduced from reference [14]: Microscopic swimmers (a) *E. Coli*, (b) *C. crescentus*. (c) *R. sphaeroides* (d) *Spiroplasma* (e) *Human spermatozoa* (f) *Mouse spermatozoa* (g) *Chlamydomonas*. (h) *Paramecium*

¹Parts of this work have been presented in the following conferences.

American Physical Society - Division of Fluid Dynamics (APS-DFD), Nov. 22 - 24, 2020, Chicago, Illinois

Coastal Bend Mathematics and Statistics Conference (CBMSC), April 10, 2021, Texas A&M University, San Antonio

As seen in Figure 1.1, commonly observed microorganisms possess geometrical shapes like that of a sphere (most frequently found), a thin rod, a spheroid, among others. In 1952, Lighthill [15] introduced the simplest possible mathematical model of a swimming microorganism as a single-celled protozoan covered with beating cilia in a purely viscous fluid-also known as the *Newtonian fluid*. This model is popularly known as *squirmers model* and has become a standard reference in subsequent studies. The model consisted of a sphere squirming with its surface oscillations (radial and tangential mode of oscillations). Blake [2], completed the calculations for the *swimming/propulsion speed, power dissipation, and swimming efficiency* of the spherical squirmer for the model introduced by Lighthill. A representative spherical microorganism squirmer model in slow viscous flow (low-Reynolds number flow) used by Lighthill and Blake is shown in Figure 1.3.

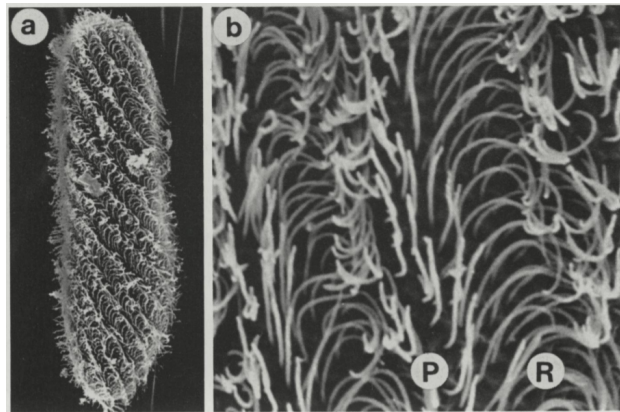


Figure 1.2
 Reproduced from reference [20]: (a) A scanning electron micrograph of *Paramecium caudatum* ($150\mu\text{m}$ long) depiction of form and orientation of cilia beating on a forward-swimming cell. (b) Detail of a region of a similar micrograph from another cell showing a prominent recovery wave R and a less obvious band of cilia in their power stroke P.

In this representative model (Figure 1.3), the radius R represents the radial distance from the origin to the maximum elongation of the cilia. Similarly, the radius a represents the *actual surface of the organism* and the surface of analysis. The angles θ and θ_0 correspond to the angular position of the maximum elongation of the cilia and the actual surface of the microorganism, respectively. The velocity U is associated with the axisymmetric flow (zero azimuthal component) of the surrounding Newtonian fluid.

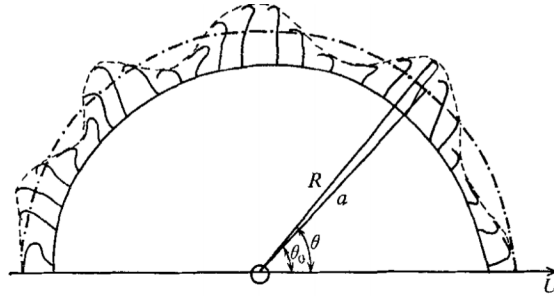


Figure 1.3

Reproduced from reference [2]: Surface oscillation/velocity represented due to the cilia beating

In the aforementioned mathematical model, the self-propulsion of the microorganism by the cilia beating is represented as the surface velocity change (oscillations) in a viscous fluid. This leads to a different set of boundary conditions (variable surface slip) compared to the Stokes flow past a solid sphere (no-slip) [11]. The classic works of Lighthill and Blake became instrumental for the currently growing subject on low Reynolds-number locomotion in a highly viscous fluid and now there is extensive literature on this topic (see [14, 17, 20] and references therein). However, less is known on the theoretical modeling of swimming mechanisms in fluid environments that depart from the classical Newtonian fluid. In this thesis, we propose to investigate the mathematical model of a squirming sphere, modeling a self-propelling microorganism, in a micropolar fluid with a goal to understand swimming mechanisms in complex fluid environments.

For a certain class of complex fluids with suspended structures such as ions, atoms, molecules, particulate matters, the classical theory of fluids does not seem to give adequate results. Several modified continuum models to describe the flow structures of complex fluids have been proposed in the literature. Eringen [7] first proposed the theory behind *micropolar fluids* and defined *as the class of fluids which exhibits micro-rotational effect and the micro-rotational inertia*. The micropolar fluids belong to a subclass of the more general polar fluids with physical aspects consisting of: rigid, randomly oriented particles suspended in a viscous medium; where the deformation of the particles is negligible. Such fluids exhibit microscopic effects due to the microstructures present in the fluid and micro-motions of the fluid-structure. The rotational part in micropolar fluids contributes to the non-symmetrical stress and the so-called couple stress. The magnitude of

the micro-rotational viscosity is what makes the micropolar fluid different from the classical Newtonian fluid. Common examples of such complex-structured fluids are human and animal blood. Liquid crystals with dumbbell shape structures can also be considered as examples of micropolar fluids. The theory of polar fluids was formulated later by [6] who defined a fluid model with two basic kinematic vector fields (velocity and spin vector fields), antisymmetric stress, symmetric stress, and couple stresses. Polar fluid models have also been applied to study blood flows, mean turbulent flows, and suspensions in lubrication theory [16].

The effect of micropolar fluid properties on the blood flow has been studied by Evangelos et al [13], in a human carotid from the perspective of the practical application. Carotid arteries are blood vessel in our neck that has two branches, one is to supply blood to the brain and the other to supply blood to our face and neck. The study includes a comparison between the flow due to microstructures present in the blood and the Newtonian fluid. The authors have shown the direct impact of micro-rotation viscosity on blood flow. One of their findings is that with the higher micropolarity values the flow velocity increases at the center of the vessels and decreases close to the boundary thereby increasing the thickness of the boundary layer. This result has led to an investigation on the effect of human health causing atherosclerosis which is caused due to the accumulation of fat and other substances on the artery walls. Also, an increase in the vortex viscosity leads to an increase in micro-rotation, which reduces the effect of shear stress on the carotid walls, thus creating high chances of accumulation of foreign substances on the walls of the carotid. This example illustrates the significance of the spin effect present in polar fluid models. In our present investigation, we examine the consequence of micro-rotation on microorganism swimming in micropolar fluids.

The fundamental mathematical problem of the slow uniform flow of a micropolar fluid past a sphere has been addressed on several occasions (see [12, 18], for instance) in order to calculate the flow fields and the drag force acting on the solid spherical surface. In those analyses, the surface velocity is either zero (no-slip condition) or a constant on the spherical surface [11]. However, for the squirming model problem under consideration, the surface velocities change periodically on

the surface of the squirmer due to the self-propulsion (Figure 1.3). The micro-rotation associated with the micropolar fluids will change as a result of the surface oscillations occurring at the spherical boundary due to cilia beating. As a result, the swimming characteristics may be affected by these additional effects. Thus there is a need for modifications in the model used by Lighthill and Blake for Newtonian Stokes fluids. Therefore, we analyze the mathematical problem of squirmer motion of a sphere in a micropolar fluid subject to surface velocity changes by mimicking Lighthill and Blake model for the Newtonian fluid. Our calculations will include the determination of the propulsion speed, power, and hydrodynamic efficiency of the swimming spherical microorganism in micropolar fluid environments.

The thesis is structured as follows: We begin with the basic model equations for the problem of microorganism swimming in micropolar fluid in **Chapter 2**. The stream function formulation of the governing equations for velocity, pressure, and micro-rotation fields in the case of axisymmetric flows is provided. The surface velocity boundary conditions similar to those used by Lighthill [15] and Blake [2] for spherical squirmer are also discussed. The chapter concludes with the derivation of general solutions of the equations satisfied by the stream function obtained in terms of spherical harmonics and modified spherical Bessel functions. In **Chapter 3**, exact analytical solutions for the sixth order PDE with velocity slip boundary conditions at the surface of a spherical squirmer. The swimming speed, power, and efficiency calculations are given in the same chapter. Detailed results for 1-mode and 2-mode problems are provided in **Chapter 4**. Expressions for the velocity components and micro-rotation are given and the reduction of our results to the classical Newtonian case is shown. The streamline plots, graphical illustrations, and numerical results are provided as well. Finally, in **Chapter 5** we summarize the key findings of our work reported in this thesis.

The symbols used in this thesis are taken from the references and are listed in the nomenclature. TAMUCC template is used as format for the thesis.

CHAPTER II: MATHEMATICAL FORMULATION

As described in the introduction, the micropolar fluid exhibits micro-rotational and micro-rotational inertia. This is in contrast to the classic Newtonian fluid where such effects are absent. The presence of micro-rotation induces non-symmetrical couple stress. As a result, the governing equations for the flow of micropolar fluid are significantly different from those for classical Newtonian fluids. In this chapter, we provide the basic mathematical equations for the flow of a micropolar fluid following the work of Eringen [8], Lukaszewicz [16] among others. For the sake of simplicity, we consider axisymmetric flows so the scalar stream function formulation can be adopted as in the case of Stokes flow. The stream function method reduces the coupled velocity and micro-rotation vector PDEs to a single sixth-order scalar PDE. The latter equation admits general solutions via the separable method suitable for linear PDEs. We also state the variable surface velocity boundary conditions for a spherical swimmer in a micropolar fluid that are used later to solve the mathematical boundary value problem. Derivation of the general solution of the sixth-order scalar PDE satisfied by the stream function is given in section 2.4 of this chapter. The general solution is used in the subsequent chapter to obtain exact results in specific cases for the swimming problem.

2.1 Basic Equations

The constitutive equations for the motion of micropolar fluid, in terms of the stress tensor T_{ij} and the couple stress tensor C_{ij} in the absence of inertia and body forces are given by [8],

$$T_{ij} = (-p + \lambda_1 \operatorname{div} \mathbf{u}) \delta_{ij} + \mu (u_{i,j} + u_{j,i}) + k (u_{j,i} - \varepsilon_{ijm} \Omega_m), \quad (2.1)$$

$$C_{ij} = (\alpha_1 \operatorname{div} \Omega) \delta_{ij} + \beta_1 \Omega_{i,j} + \gamma \Omega_{j,i}, \quad (2.2)$$

where p , \mathbf{u} , Ω , are the pressure, velocity vector, and micro-rotation vector, respectively. Here μ , k and λ_1 are the material constants. Also, $\mu = \nu - \nu_r$ and $k = 2\nu_r$ in terms of the classical Newtonian viscosity (ν) and rotational viscosity (ν_r) as explained in Hoffmann [12]. The notations δ_{ij} and $\varepsilon_{j pq}$ correspond to Kronecker delta and permutation symbol, respectively. The additional constants α_1, β_1 and γ are known as angular viscosity coefficients. Note that in equations (2.1) and (2.2) mixed notations are adopted to distinguish tensors and vectors for the sake of convenience. The

term $k(u_{j,i} - \varepsilon_{j pq} \Omega_m)$ contributes to the anti-symmetric part for the stress tensor in equation (2.1). For $k = \nu_r = 0$, equation (2.1) reduces to

$$T_{ij} = (-p + \lambda_1 \operatorname{div} \mathbf{u}) \delta_{ij} + \mu(u_{i,j} + u_{j,i}),$$

which yields the stress tensor for the Newtonian fluid (with non-zero divergence). Note that equation (2.2) is irrelevant in this case.

In our swimming problem, we assume the micropolar fluid to be incompressible and the flow is steady. Under these conditions, the constitutive equations (2.1) and (2.2) describing the motion for slow flow of an incompressible micropolar fluid in terms of velocity, pressure, and micro-rotation, can be written in the form [16],

$$-(\mu + k)(\operatorname{curl} \operatorname{curl} \mathbf{u}) + k(\operatorname{curl} \Omega) = \operatorname{grad} p, \quad (2.3)$$

$$-\gamma(\operatorname{curl} \operatorname{curl} \Omega) + k(\operatorname{curl} \mathbf{u}) - 2k\Omega = 0. \quad (2.4)$$

The incompressibility condition or the continuity equation is given by,

$$\operatorname{div} \mathbf{u} = 0. \quad (2.5)$$

Equations (2.3), (2.4), and (2.5) represent the vector PDEs governing the steady motion of an incompressible micropolar fluid. The boundary value problems for vector PDEs are hard to deal with and therefore, we restrict the flow to be axisymmetric to simplify our analysis. In the following section, we describe the reduction of governing equations for axisymmetric flows in spherical coordinates.

2.2 Axisymmetric Flow in Spherical Polar Coordinates

First, we choose O as the origin of the Cartesian frame as in Figure 2.4 and $P(x, y, z)$ be a point with coordinates x, y, z . Let r, θ, ϕ be the spherical polar coordinates as shown in the Figure 2.4 with $0 \leq r < \infty, 0 \leq \theta \leq \pi, 0 \leq \phi \leq 2\pi$.

Let $\hat{\mathbf{e}}_r, \hat{\mathbf{e}}_\theta$ and $\hat{\mathbf{e}}_\phi$ be the unit vectors along the radial, transverse and azimuthal directions, respectively (see Figure 2.4). The transformation between the Cartesian and spherical coordinates is

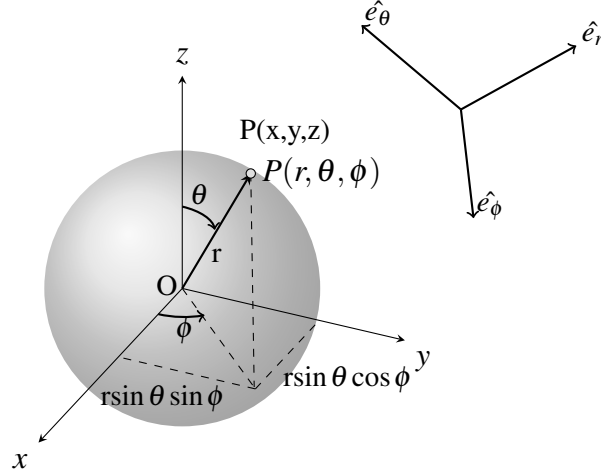


Figure 2.4
Spherical Polar Coordinates System

given by

$$x = r \sin \theta \cos \phi, \quad y = r \sin \theta \sin \phi, \quad z = r \cos \theta,$$

and the inverse transformation (from spherical to cartesian) is

$$r^2 = x^2 + y^2 + z^2, \quad \tan \theta = \frac{\sqrt{x^2 + y^2}}{z}, \quad \tan \phi = \frac{y}{x}.$$

For **axisymmetric flows**, all the physical quantities are independent of the azimuthal angle ϕ and further $u_\phi = 0$. Thus, the spherical velocity components u_r , u_θ and $u_\phi = 0$ and the micro-rotation components Ω_r , Ω_θ and Ω_ϕ depend only on r and θ . In this case, the velocity vector \mathbf{u} takes the form

$$\mathbf{u}(r, \theta) = u_r(r, \theta) \hat{\mathbf{e}}_r + u_\theta(r, \theta) \hat{\mathbf{e}}_\theta. \quad (2.6)$$

The continuity equation (2.5) implies that u_r and u_θ can be derived from a single scalar function, known as the Stokes stream function, $\psi(r, \theta)$ [12, 17, 18] as follows,

$$u_r(r, \theta) = -\frac{1}{r^2 \sin \theta} \frac{\partial \psi}{\partial \theta} \quad (2.7)$$

$$u_\theta(r, \theta) = \frac{1}{r \sin \theta} \frac{\partial \psi}{\partial r} \quad (2.8)$$

Now the equations (2.3) and (2.4) can be rewritten in the form

$$\text{grad } p = -\frac{1}{2}(2\mu + k)\text{curl curl } \mathbf{u} - \frac{\gamma(\mu + k)}{2k}\text{curl curl curl curl } \mathbf{u}, \quad (2.9)$$

$$\Omega = \frac{1}{2}\text{curl } \mathbf{u} - \frac{\gamma(\mu + k)}{2k^2}\text{curl curl curl } \mathbf{u}. \quad (2.10)$$

Note that the velocity and micro-rotation vectors are decoupled in the above forms of the governing equations for micropolar fluids. Eliminating the pressure in (2.9) results in

$$\text{curl curl curl curl curl } \mathbf{u} + \left(\frac{k(2\mu + k)}{\gamma(\mu + k)} \right) \text{curl curl curl } \mathbf{u} = 0. \quad (2.11)$$

Equivalently, using the vector identity $\text{curl curl } \mathbf{u} = \text{grad div } \mathbf{u} - \nabla^2 \mathbf{u}$, one obtains

$$\text{curl } (\nabla^4 \mathbf{u} - \delta^2 \nabla^2 \mathbf{u}) = 0, \quad (2.12)$$

where the parameter δ^2 is defined as

$$\delta^2 = \frac{2k}{\gamma(1 + \varepsilon)}, \quad \varepsilon = \frac{k}{(2\mu + k)}.$$

Using (2.7) and (2.8), the $\text{curl } \mathbf{u}$ is computed in terms of Stokes stream function as

$$\text{curl } \mathbf{u} = \frac{1}{r \sin \theta} \left[\frac{\partial^2 \psi}{\partial r^2} + \frac{1}{r^2} \frac{\partial^2 \psi}{\partial \theta^2} - \frac{\cot \theta}{r^2} \frac{\partial \psi}{\partial \theta} \right] \hat{\mathbf{e}}_\phi. \quad (2.13)$$

The use of (2.13) in (2.12) and after some simplification we get the following **sixth-order** PDE for the Stokes stream function in the form

$$E^4(E^2 \psi - \delta^2 \psi) = 0, \quad (2.14)$$

where the axisymmetric Stokes operator E^2 is defined as

$$E^2 = \frac{\partial^2}{\partial r^2} + \frac{1}{r^2} \frac{\partial^2}{\partial \theta^2} - \frac{\cot \theta}{r^2} \frac{\partial}{\partial \theta}.$$

Again, using (2.3) and (2.4), the non-vanishing ϕ - component of the micro-rotation vector Ω can be represented in terms of the Stokes-stream function as

$$\Omega(r, \theta) = \frac{1}{2r \sin \theta} \left\{ E^2 \psi + \frac{1}{\delta^2 \varepsilon} E^4 \psi \right\} \hat{\mathbf{e}}_\phi. \quad (2.15)$$

Once again we point out that in the limit of $k, \gamma \rightarrow 0$, equations (2.3), (2.4) and (2.5) reduce to the **Stokes equations** for the Newtonian fluid given by

$$\mu \nabla^2 \mathbf{u} = \text{grad } p, \quad \nabla \cdot \mathbf{u} = 0.$$

In the next section we state the boundary conditions for a spherical squirmer in a micropolar fluid.

2.3 Boundary Conditions for Spherical Squirmer

The schematic of the axisymmetric flow configuration for a spherical squirmer model in a micropolar fluid is shown in Figure 2.5. For spherical squirmer models, the surface velocities change periodically due to self-propelling mechanisms of the micro-organisms. The boundary conditions in this case (on the squirmer surface $r = a$), as suggested in [2, 15], take the form

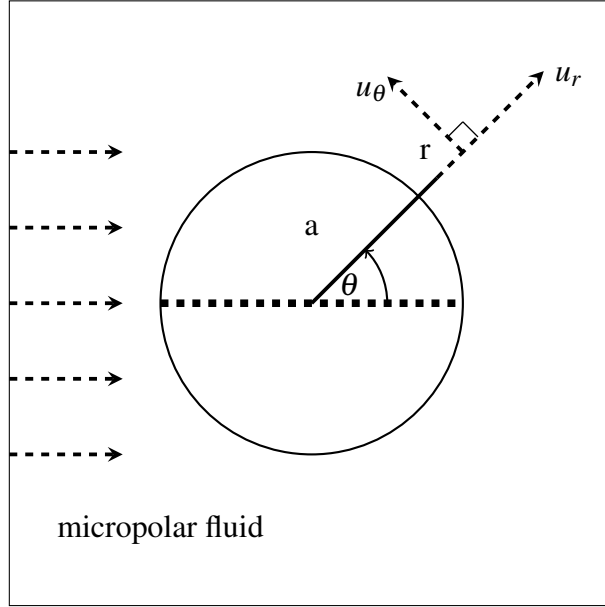


Figure 2.5
Representation of spherical microorganism placed in a micropolar fluid

$$u_r(a, \theta) = \sum_{n=0}^{\infty} A_n P_n(\cos \theta), \quad u_\theta(a, \theta) = \sum_{n=1}^{\infty} B_n V_n(\cos \theta). \quad (2.16)$$

In the above equation,

$$V_n(\cos \theta) = -\frac{2}{n(n+1)} P_n^1(\cos \theta),$$

where $P_n(\cos \theta)$ and $P_n^1(\cos \theta)$ are the Legendre polynomial and the associated Legendre polynomial of the first kind, respectively. The coefficients A_n and B_n correspond to the radial and tangential modes of oscillations. It should be noted that the surface velocity conditions (2.16) can be readily transformed in terms of the stream function by the use of (2.7) and (2.8).

Thus, the spherical squirmer model in micropolar fluids reduces to solving the mathematical boundary value problem (BVP) for the stream function satisfying (2.14) subject to the surface velocity boundary conditions given in (2.16). It has been shown in [2, 15] that only the first mode A_1 and B_1 (for $n = 1$) contribute to the swimming speed/velocity of the spherical squirmer while the power and efficiency depend on all the A_n and B_n modes in the case of Stokes flow. We show in **Chapter 3** that this conclusion holds for micropolar fluids as well.

The non-zero boundary condition for micro-rotation at the surface of the spherical squirmer ($r = a$) is taken to be [12]

$$\Omega = \frac{\alpha}{2} \text{curl } \mathbf{u} \quad \text{with } 0 \leq \alpha \leq 1 \quad \text{at } r = a. \quad (2.17)$$

When the constants A_n, B_n and α (non-zero micro-rotation) are zero, the above boundary condition in vector form reduces to the no-slip condition considered in [18] for the translational drag problem for a sphere placed in a micropolar fluid.

The scalar boundary value problem formulated here will be utilized in the next chapter to obtain exact solutions for the stream function including a variety of modes. The velocity and micro-rotation components are then computed using (2.7), (2.8), and (2.15) via, a straightforward differentiation process. Below we record the derivation of the general solution of the sixth-order PDE (2.14) satisfied by the stream function in spherical coordinates.

2.4 Derivation of the General Solutions

This section provides the derivation for the general solution to the sixth-order PDE (2.14) using the separation of variables and variation of parameters. The linearity allows us to decompose (2.14) in the form

$$(E^2 - \delta^2)v = 0, \quad (2.18)$$

and

$$E^4 \chi = 0, \quad (2.19)$$

where the axisymmetric operator E^2 is defined in the section 2.2 (see the equation below (2.14)). The classical method to solve the sixth-order PDE is to split the whole equation as in (2.18)-(2.19). Using the principle of superposition for linear PDEs, the general solution ψ can be represented as $\psi = v + \chi$. Notice that v satisfies the homogeneous axisymmetric Helmholtz equation (2.18) and χ satisfies the homogeneous axisymmetric biharmonic equation (2.19). We first solve the Helmholtz equation (2.18) using the *separation of variables*. Thus,

$$v(r, \theta) = R(r)\Theta(\theta). \quad (2.20)$$

Substitution of (2.20) in (2.18) yields the following

$$\frac{R''}{R} + \frac{1}{r^2} \frac{\Theta''}{\Theta} - \frac{\cot \theta}{r^2} \frac{\Theta'}{\Theta} - \delta^2 = 0, \quad (2.21)$$

which can be written in the form

$$r^2 \frac{R''}{R} - \delta^2 r^2 = -\frac{\Theta''}{\Theta} + \cot \theta \frac{\Theta'}{\Theta} = n(n+1). \quad (2.22)$$

Equation (2.22) leads to the following ordinary differential equations for $R(r)$ and $\Theta(\theta)$

$$r^2 R'' - (\delta^2 r^2 + n(n+1))R = 0, \quad (2.23)$$

$$\Theta'' - \Theta' \cot \theta + n(n+1)\Theta = 0. \quad (2.24)$$

To solve the angular part of the equation (2.24) we use $x = \cos \theta$ and obtain the transformed equation in the form

$$(1-x^2) \frac{d^2 \Theta}{dx^2} + n(n+1)\Theta(x) = 0. \quad (2.25)$$

Equation (2.25) may be transformed using the substitution

$$\Theta(x) = \sqrt{1-x^2} v(x). \quad (2.26)$$

The resulting equation (after simplification) can be written as

$$\frac{d}{dx} \left[(1-x^2) \frac{dv}{dx} \right] + \left(n(n+1) - \frac{1}{\sqrt{1-x^2}} \right) v = 0. \quad (2.27)$$

Note that the transformed equation (2.27) is a special case of Sturm-Liouville equation whose solution is

$$v(x) = P_n^1(x), \quad (2.28)$$

where $P_n^1(x)$ is the associated Legendre polynomial of order 1. Now the solution to (2,25) is

$$\Theta(\theta) = \begin{cases} \sin \theta P_n^1(\cos \theta) & n \geq 1, \\ (g_0 \cos \theta + j_0) & n = 0, \end{cases} \quad (2.29)$$

where g_0 and j_0 are arbitrary constants. Next, to solve (2.23) for the radial part we use the following transformation

$$R(r) = \frac{r}{\delta^{\frac{3}{2}}} t(\delta r), \quad (2.30)$$

and transform the equation in the form

$$\frac{d}{d(\delta r)} \left((\delta r)^2 \frac{dt(\delta r)}{d(\delta r)} \right) - ((\delta r)^2 + n(n+1)) t(\delta r) = 0. \quad (2.31)$$

We now use the following change of variable

$$z = \delta r, \quad (2.32)$$

and transform the derivatives via the relations δr

$$\begin{aligned} \frac{dz}{d(\delta r)} &= 1, \\ \frac{dt}{d(\delta r)} &= \frac{dt}{dz} \frac{dz}{d(\delta r)} = \frac{dt}{dz}, \\ \frac{d^2 t}{d(\delta r)^2} &= \left(\frac{d}{dz} \frac{dz}{d(\delta r)} \right) \left(\frac{dt}{dz} \right) = \frac{d^2 t}{dz^2}. \end{aligned} \quad (2.33)$$

Simplifying (2.31) after making the above substitutions/changes we arrive at

$$\frac{d}{dz} \left(z^2 \left(\frac{dt}{dz} \right) \right) - (z^2 + n(n+1)) t = 0. \quad (2.34)$$

Equation (2.34) is a modified spherical Bessel equation whose solution is given in [1] in the form

$$t(\delta r) = \sum_{n=1}^{\infty} \frac{1}{\sqrt{\delta r}} \left(E_n I_{n+\frac{1}{2}}(\delta r) + F_n K_{n+\frac{1}{2}}(\delta r) \right). \quad (2.35)$$

where $I_{n+1/2}(\delta r)$ and $K_{n+1/2}(\delta r)$ are the modified spherical Bessel functions of the first and third kinds [1], respectively. Substitution of the above results in (2.30) yields the general solution to the radial part as

$$R(r) = \begin{cases} \left(\frac{\sqrt{r}}{\delta^2} \right) \sum_{n=1}^{\infty} \left(E_n I_{n+\frac{1}{2}}(\delta r) + F_n K_{n+\frac{1}{2}}(\delta r) \right) & \text{for } n \geq 1, \\ e_0 e^{\delta r} + f_0 e^{-\delta r} & \text{for } n = 0, \end{cases} \quad (2.36)$$

where E_n , F_n , e_0 , and f_0 are arbitrary constants. Thus, the solution to the axisymmetric Helmholtz equation (2.18) (after combining the radial and angular parts) becomes

$$\begin{aligned} v(r, \theta) = & \left(e_0 e^{\delta r} + f_0 e^{-\delta r} \right) (g_0 \cos \theta + j_0) \\ & + \left(\frac{\sqrt{r}}{\delta^2} \right) \sum_{n=1}^{\infty} \left[\left(E_n I_{n+\frac{1}{2}}(\delta r) + F_n K_{n+\frac{1}{2}}(\delta r) \right) \right] \sin \theta P_n^1(\cos \theta). \end{aligned} \quad (2.37)$$

The general solution to the axisymmetric biharmonic equation (2.19) may be derived as follows. Using the linearity property, equation (2.19) can be split in the form

$$E^2 \chi_h = 0, \quad (2.38)$$

and

$$E^2 \chi_p = \chi_h, \quad (2.39)$$

where we have used

$$\chi(r, \theta) = \chi_h(r, \theta) + \chi_p(r, \theta). \quad (2.40)$$

Note that $\chi_h(r, \theta)$ satisfies the homogeneous axisymmetric Laplace equation and $\chi_p(r, \theta)$ is a solution of the nonhomogeneous (axisymmetric) Laplace equation. We solve equation (2.38) using the separation of variables, and so let

$$\chi_h(r, \theta) = R_h(r) \Theta_h(\theta). \quad (2.41)$$

This substitution yields the following two ordinary differential equations

$$r^2 R_h'' + \lambda R_h = 0, \quad (2.42)$$

$$\Theta_h'' - \cot(\theta)\Theta_h' - \lambda\Theta_h = 0. \quad (2.43)$$

Taking the eigenvalue $\lambda = -n(n+1)$ and solving (2.42) and (2.43), we obtain the solution for $\chi_h(r, \theta)$ in the form

$$\chi_h(r, \theta) = (a_0 + b_0 r)(g_0 \cos \theta + j_0) + \sum_{n=1}^{\infty} (C_n r^{-n} + B_n r^{n+1}) \sin \theta P_n^1(\cos \theta), \quad (2.44)$$

where a_0, b_0, C_n, B_n are arbitrary constants. Using (2.44) one can solve the nonhomogeneous Laplace equation (2.39) by the method of *separation of variables* (for the homogeneous part) and the *variation of parameters* technique (for the particular solution). The general solution of the homogeneous part (2.44) will be considered further to derive the particular solution. Thus, two cases arise which we address separately.

CASE I: n=0 (Degenerate Case)

Let $y_1(r) = 1$ and $y_2(r) = r$ be the solutions of the corresponding homogeneous differential equation. Then, the Wronskian for $W(y_1(r), y_2(r)) = 1$. Now a particular solution is taken as

$$\chi_{1p}(r, \theta) = R_p(r)\Theta_p(\theta),$$

where

$$R_p(r) = -y_1(r) \int \frac{y_2(r)f(r)}{W(y_1, y_2)} dr + y_2(r) \int \frac{y_1(r)f(r)}{W(y_1, y_2)} dr,$$

where $f(r) = a_0 + b_0 r$, and $\Theta_p(\theta) = (g_0 \cos \theta + j_0)$.

Evaluating the integrals we obtain a particular solution for $n = 0$ in the form

$$\chi_{1p}(r, \theta) = (a_0 + b_0 r + c_0 r^2 + d_0 r^3)(g_0 \cos \theta + j_0),$$

where c_0 and d_0 are arbitrary constants.

CASE II: $n \geq 1$

Let $y_1(r) = r^{-n}$ and $y_2(r) = r^{n+1}$ be two linearly independent solutions of the corresponding homogeneous differential equation and the Wronskian is $W(y_1, y_2) = 2n + 1$.

We assume a particular solution as

$$\chi_{2p}(r, \theta) = R_p(r)\Theta_p(\theta), \quad (2.45)$$

where

$$R_p(r) = -y_1(r) \int \frac{y_2(r)f(r)}{W(y_1, y_2)} dr + y_2(r) \int \frac{y_1(r)f(r)}{W(y_1, y_2)} dr, \quad (2.46)$$

$$f(r) = \sum_{n=1}^{\infty} (C_n r^{-n} + B_n r^{n+1}) \text{ and}, \quad (2.47)$$

$$\Theta_p(\theta) = \sin \theta P_n^1(\cos \theta), \quad (2.48)$$

Solving for R_p , we get

$$R_p(r) = \sum_{n=1}^{\infty} \left(A_n r^{n+3} + \frac{D_n}{r^{n-2}} \right). \quad (2.49)$$

Therefore, we obtain the particular solution as,

$$\chi_{2p}(r, \theta) = \sum_{n=1}^{\infty} \left(A_n r^{n+3} + \frac{D_n}{r^{n-2}} \right) \sin \theta P_n^1(\cos \theta). \quad (2.50)$$

Recalling the equation for χ_p ,

$$\chi_p = \chi_{1p} + \chi_{2p}.$$

Substituting the results for $\chi_h(r, \theta)$ and $\chi_p(r, \theta)$ into the equation (2.40), one gets

$$\begin{aligned} \chi(r, \theta) &= (a_0 + b_0 r + c_0 r^2 + d_0 r^3) (g_0 \cos \theta + j_0) \\ &+ \sum_{n=1}^{\infty} \left(A_n r^{n+3} + B_n r^{n+1} + \frac{C_n}{r^n} + \frac{D_n}{r^{n-2}} \right) \sin \theta P_n^1(\cos \theta). \end{aligned} \quad (2.51)$$

Combining the solutions of (2.18) and (2.19) derived above we obtain the general solution of the PDE (2.14) in the following form

$$\begin{aligned} \psi(r, \theta) = & \left(a_0 + b_0 r + c_0 r^2 + d_0 r^3 + e_0 e^{\delta r} + f_0 e^{-\delta r} \right) (g_0 \cos \theta + j_0) \\ & + \sum_{n=1}^{\infty} \left[a_n r^{n+3} + b_n r^{n+1} + \frac{C_n}{r^n} + \frac{D_n}{r^{n-2}} + \frac{\sqrt{r}}{\delta^2} \left(E_n I_{n+\frac{1}{2}}(\delta r) + F_n K_{n+\frac{1}{2}}(\delta r) \right) \right] \sin \theta P_n^1(\cos \theta). \end{aligned} \quad (2.52)$$

Substitution of (2.53) in (2.15) yields the micro-rotation as

$$\begin{aligned} \Omega(r, \theta) = & \left(2c_0 + 6d_0 r + \delta^2 \left(\frac{1+\varepsilon}{\varepsilon} \right) \left(e_0 e^{\delta r} + f_0 e^{-\delta r} \right) \right) (g_0 \cos \theta + j_0) \\ & + \sum_{n=1}^{\infty} \left[2(2n+3)a_n r^n - \frac{2(2n-1)D_n}{r^{n+1}} + \left(\frac{1+\varepsilon}{2\varepsilon} \right) \frac{1}{\sqrt{r}} \left(E_n I_{n+\frac{1}{2}}(\delta r) + F_n K_{n+\frac{1}{2}}(\delta r) \right) \right] P_n^1(\cos \theta). \end{aligned} \quad (2.53)$$

We point out that the terms due to $n = 0$ do not contribute to the swimming problem under consideration. Therefore, we take $n \geq 1$ terms in the general solutions above. For the freely swimming sphere with the mean speed U in micropolar fluid we add the term $\frac{U}{2} r^2 \sin^2(\theta)$ in the stream function.

Further, the finite velocity requirement as $r \rightarrow \infty$ implies $a_n = b_n = E_n = 0$. Finally, the solutions for the stream function and the micro-rotation for the squirming sphere in the micropolar fluid are taken to be

$$\begin{aligned} \psi(r, \theta) = & \frac{U}{2} r^2 \sin^2 \theta - \left(\frac{C_1}{r} + D_1 r + \frac{\sqrt{r}}{\delta^2} F_1 k_{\frac{3}{2}}(\delta r) \right) \sin^2 \theta \\ & + \sum_{n=2}^{\infty} \left(\frac{C_n}{r^n} + \frac{D_n}{r^{n-2}} + \frac{\sqrt{r}}{\delta^2} F_n K_{n+\frac{1}{2}}(\delta r) \right) \sin \theta P_n^1(\cos \theta) \end{aligned} \quad (2.54)$$

and,

$$\begin{aligned} \Omega(r, \theta) = & \left(\frac{D_1}{r^2} - \left(\frac{1+\varepsilon}{2\varepsilon} \right) \frac{F_1}{\sqrt{r}} K_{\frac{3}{2}}(\delta r) \right) \sin \theta \\ & + \sum_{n=1}^{\infty} \left[-\frac{2(2n-1)D_n}{r^{n+1}} + \left(\frac{1+\varepsilon}{2\varepsilon} \right) \frac{F_n}{\sqrt{r}} K_{n+\frac{1}{2}}(\delta r) \right] P_n^1(\cos \theta). \end{aligned} \quad (2.55)$$

The general solutions (2.54) and (2.55) will be used in the next chapter to derive exact results for a spherical squirmer suspended in micropolar fluids.

CHAPTER III: TWO-MODE AND n -MODE ANALYTICAL SOLUTIONS FOR A SPHERICAL SQUIRMER

The scalar stream function formulation of the spherical squirmer in micropolar fluid problem stated in (2.14) subject to the surface velocity slip conditions (2.16) and the non-zero microrotation condition (2.17) will now be used to generate closed-form analytical solutions. For the sake of clarity, we record the calculations for the 2-Mode and n -Mode solutions separately. We emphasize that the determination of the stream function provides a basis for the discussion of the flow fields prevailing in the presence of a squirmer. By a direct differentiation process, one can obtain the radial and tangential velocity components via the relations given in (2.7) and (2.8). These necessary quantities are required for the swimming speed, power, and efficiency calculations of the squirming sphere in micropolar fluids modeled by the equations (2.3) - (2.5). The pressure can be obtained by direct integration of (2.9) while the micro-rotation is derived using (2.15) (or equivalently, using (2.10)). The essential steps used in the derivation of swimming speed, power, and efficiency due to the swimming of a spherical squirmer in a micropolar fluid are summarized below.

- Use the stream function (2.54) and micro-rotation (2.55) as suitable solutions for the swimming problem under consideration. Note that, as in the case of swimming in Newtonian fluids [2, 15], these choices satisfy the requirement that the induced velocity and the micro-rotation must be finite at large distances from the spherical squirmer.
- Apply the non-vanishing surface velocity and micro-rotation boundary conditions (2.16) and (2.17), respectively, to determine the unknown arbitrary constants in the stream function for various radial and tangential modes. Due to the linearity of the governing equations, 2-Mode and n -Mode cases can be treated separately.
- Find the radial and tangential velocity components via direct differentiation using (2.7) and (2.8).
- Compute pressure using (2.9) and stress components using (3.77), (3.78) and (3.81).

- Integrate stress components to find drag on the surface of the spherical squirmer (use (3.85)).
- Use force-free condition to obtain the swimming speed [2, 15].
- Determine the power using (3.93). This requires the integration of the product of velocity and stress components on the surface of the squirmer. Calculate the efficiency via the relation given in (3.97).

The aforementioned steps are utilized to determine the relevant physical quantities of interest in the context of squirming motion of a sphere in micropolar fluids in the next sections. The essential quantities computed here are employed to understand the swimming characteristics in **Chapter 4**.

3.1 Two-Mode Results for the Stream function, Velocity, Micro-rotation and Stress Components

From (2.54), the stream function for the 2-mode solution can be written as

$$\begin{aligned} \psi^{2M}(r, \theta) = & \frac{Ur^2}{2} \sin^2 \theta - \left(\frac{C_1}{r} + D_1 r + \frac{\sqrt{r}}{\delta^2} F_1 k_{\frac{3}{2}}(\delta r) \right) \sin^2 \theta \\ & - 3 \left(\frac{C_2}{r^2} + D_2 + \frac{\sqrt{r}}{\delta^2} F_2 K_{\frac{5}{2}}(\delta r) \right) \sin^2 \theta \cos \theta. \end{aligned} \quad (3.56)$$

The boundary conditions for the 2-mode are

$$u_r^{2M}(a, \theta) = A_1 \cos \theta + \frac{A_2}{2} (3 \cos^2 \theta - 1), \quad (3.57)$$

$$u_\theta^{2M}(a, \theta) = B_1 \sin \theta + B_2 \sin \theta \cos \theta, \quad (3.58)$$

$$\Omega^{2M}(a, \theta) = \frac{\alpha}{2} \text{curl } \mathbf{u}^{2M}. \quad (3.59)$$

Computing the fluid velocity components using (3.56), (2.7) and (2.8), and the micro-rotation from (2.55) require the use of the recurrence relations and differentiation properties of the modified spherical Bessel function $K_{n+\frac{1}{2}}(\delta r)$ that are mentioned in *Appendix A*,

$$\begin{aligned} u_r^{2M}(r, \theta) = & -U \cos \theta + \left(\frac{2C_1}{r^3} + \frac{2D_1}{r} + \frac{2F_1}{\delta^2 r^{\frac{3}{2}}} K_{\frac{3}{2}}(\delta r) \right) \cos \theta \\ & + 3 \left(\frac{C_2}{r^4} + \frac{D_2}{r^2} + \frac{F_2}{\delta^2 r^{\frac{3}{2}}} K_{\frac{5}{2}}(\delta r) \right) (3 \cos^2 \theta - 1), \end{aligned} \quad (3.60)$$

$$u_{\theta}^{2M}(r, \theta) = U \sin \theta + \left(\frac{C_1}{r^3} - \frac{D_1}{r} + \frac{F_1}{\delta^2 r^{\frac{3}{2}}} (\delta r K_{\frac{1}{2}}(\delta r) + K_{\frac{3}{2}}(\delta r)) \right) \sin \theta + 3 \left(\frac{2C_2}{r^4} + \frac{F_2}{\delta^2 r^{\frac{3}{2}}} (\delta r K_{\frac{3}{2}}(\delta r) + 2K_{\frac{5}{2}}(\delta r)) \right) \sin \theta \cos \theta, \quad (3.61)$$

$$\Omega^{2M}(r, \theta) = \left(\frac{D_1}{r^2} - \left(\frac{1+\varepsilon}{2\varepsilon} \right) \frac{F_1}{\sqrt{r}} K_{\frac{3}{2}}(\delta r) \right) \sin \theta + 3 \left(\frac{3D_2}{r^2} - \left(\frac{1+\varepsilon}{2\varepsilon} \right) \frac{F_2}{\sqrt{r}} K_{\frac{5}{2}}(\delta r) \right) \sin \theta \cos \theta. \quad (3.62)$$

The constants in the 2-mode solution are determined using the boundary conditions (3.57)-(3.59) and are given by

$$C^{2M} = C_1 + C_2, \quad (3.63)$$

where

$$C_1 = -\frac{a^3}{4} \left[\frac{(1-\alpha) \varepsilon (3U - 2B_1 + A_1)}{\Lambda_1} \left(1 + 2 \left(\frac{1}{\delta a} + \frac{1}{\delta^2 a^2} \right) \right) + (U - 2B_1 - A_1) \right], \quad (3.64)$$

$$C_2 = \frac{a^4}{6} \left[B_2 + \frac{3(1-\alpha) \varepsilon (B_2 - A_2)}{\Lambda_2} \left(1 + \delta a + 2 \left(1 + \frac{3}{\delta a} + \frac{3}{\delta^2 a^2} \right) \right) \right], \quad (3.65)$$

$$F^{2M} = F_1 + F_2, \quad (3.66)$$

where

$$F_1 = \frac{e^{\delta a}}{\sqrt{2\pi\delta a}} \left(\frac{(3U - 2B_1 + A_1) (1-\alpha) \varepsilon \delta^2 a^{\frac{3}{2}}}{\Lambda_1} \right), \quad (3.67)$$

$$F_2 = -\frac{e^{\delta(a)}}{\sqrt{2\pi\delta a}} \left(\frac{2(B_2 - A_2) (1-\alpha) \varepsilon \delta^3 a^{\frac{5}{2}}}{\Lambda_2} \right), \quad (3.68)$$

$$D^{2M} = D_1 + D_2, \quad (3.69)$$

where

$$D_1 = \frac{(3U - 2B_1 + A_1)a}{4} \left(1 + \frac{(1-\alpha) \varepsilon}{\Lambda_1} \right), \quad (3.70)$$

$$D_2 = -\frac{(B_2 - A_2)a^2}{6} \left(1 + \frac{3(1-\alpha) \varepsilon (1 + \delta a)}{\Lambda_2} \right). \quad (3.71)$$

also,

$$\begin{aligned}\Lambda_1 &= \delta a(1 + \varepsilon(1 - \alpha)) + 1, \\ \Lambda_2 &= \delta^2 a^2(1 + \varepsilon(1 - \alpha)) + 3(1 + \delta a).\end{aligned}$$

Substituting (3.63) - (3.71) in (3.60) - (3.62) we obtain the velocity and micro-rotation components for a 2-mode model in micropolar fluid in the form

$$\begin{aligned}u_r^{2m}(r, \theta) &= -U \cos \theta + \left[\frac{(3U - 2B_1 + A_1)}{2} \left(1 + \frac{(1 - \alpha)\varepsilon}{\Lambda_1} \right) \left(\frac{a}{r} - \frac{a^3}{r^3} \right) \right. \\ &\quad \left. - \frac{(3U - 2B_1 + A_1)(1 - \alpha)\varepsilon}{\Lambda_1} \left(\frac{a^3}{r^3} \left(\frac{1}{\delta a} + \frac{1}{\delta^2 a^2} \right) - \frac{ae^{\delta(a-r)}}{r} \left(\frac{1}{\delta r} + \frac{1}{\delta^2 r^2} \right) \right) \right. \\ &\quad \left. + (U + A_1) \left(\frac{a^3}{r^3} \right) \right] \cos \theta \\ &\quad + \left[\frac{(B_2 - A_2)}{2} \left(1 + \frac{3(1 - \alpha)\varepsilon(1 + \delta a)}{\Lambda_2} \right) \left(\frac{a^4}{r^4} - \frac{a^2}{r^2} \right) + \frac{A_2}{2} \left(\frac{a^4}{r^4} \right) \right. \\ &\quad \left. + \frac{3(B_2 - A_2)(1 - \alpha)\varepsilon}{\Lambda_2} \left\{ \left(1 + \frac{3}{\delta a} + \frac{3}{\delta^2 a^2} \right) \frac{a^4}{r^4} - \frac{a^2 e^{\delta(a-r)}}{r^2} \left(1 + \frac{3}{\delta r} + \frac{3}{\delta^2 r^2} \right) \right\} \right] (3 \cos^2 \theta - 1),\end{aligned}\tag{3.72}$$

$$\begin{aligned}u_\theta^{2m}(r, \theta) &= U \sin \theta \\ &\quad + \left[\frac{(3U - 2B_1 + A_1)}{4} \left(1 - \frac{(1 - \alpha)\varepsilon}{\Lambda_1} \right) \left(\frac{a^3}{r^3} \right) - \frac{(3U - 2B_1 + A_1)}{4} \left(1 + \frac{(1 - \alpha)\varepsilon}{\Lambda_1} \right) \left(\frac{a}{r} \right) \right. \\ &\quad \left. - \frac{(3U - 2B_1 + A_1)(1 - \alpha)\varepsilon}{2\Lambda_1} \left(\frac{a^3}{r^3} \left(\frac{1}{\delta a} + \frac{1}{\delta^2 a^2} \right) - \frac{ae^{\delta(a-r)}}{r} \left(1 + \frac{1}{\delta r} + \frac{1}{\delta^2 r^2} \right) \right) \right. \\ &\quad \left. + (-U + B_1) \left(\frac{a^3}{r^3} \right) \right] \sin \theta \\ &\quad + \left[B_2 \left(\frac{a^4}{r^4} \right) + \frac{3(B_2 - A_2)(1 - \alpha)\varepsilon}{\Lambda_2} \left(\frac{a^2}{r^2} \right) \left(\frac{a^2}{r^2} (1 + \delta a) - e^{\delta(a-r)} (1 + \delta r) \right) \right. \\ &\quad \left. + \frac{6(B_2 - A_2)(1 - \alpha)\varepsilon a^2}{r^2 \Lambda_2} \left(\left(\frac{a^2}{r^2} \right) \left(1 + \frac{3}{\delta a} + \frac{3}{\delta^2 a^2} \right) - e^{\delta(a-r)} \left(1 + \frac{3}{\delta r} + \frac{3}{\delta^2 r^2} \right) \right) \right] \cos \theta \sin \theta,\end{aligned}\tag{3.73}$$

$$\begin{aligned} \Omega^{2m}(r, \theta) = & \frac{(3U - 2B_1 + A_1)}{4} \left(\frac{a}{r^2}\right) \left[1 + \frac{(1 - \alpha) \varepsilon}{\Lambda_1} \left(1 - \left(\frac{1 + \varepsilon}{\varepsilon}\right) e^{\delta(a-r)}(1 + \delta r) \right) \right] \sin \theta \\ & - \frac{3(B_2 - A_2)a^2}{2r^3} \left[1 + \frac{(1 - \alpha) \varepsilon}{\Lambda_2} \left(3(1 + \delta a) - \left(\frac{1 + \varepsilon}{\varepsilon}\right) (e^{\delta(a-r)})(\delta^2 r^2 + 3\delta r + 3) \right) \right] \cos \theta \sin \theta. \end{aligned} \quad (3.74)$$

The hydrodynamic pressure is computed by substituting the equations (3.72)-(3.74) in (2.9) of **Chapter 2** and is given by

$$p^{2M}(r, \theta) = (2\mu + k) \left[\frac{D_1 \cos \theta}{r^2} + \frac{3D_2}{r^3} (3 \cos^2 \theta - 1) \right] + p_\infty. \quad (3.75)$$

Using the results for D_1 and D_2 and after simplification, one finds

$$\begin{aligned} p^{2M}(r, \theta) = & (2\mu + k) \left(\frac{a}{r^2}\right) \left[\frac{(3U - 2B_1 + A_1)}{4} + \left(\frac{(3U - 2B_1 + A_1) (1 - \alpha) \varepsilon}{4\Lambda_1} \right) \right] \cos \theta \\ & - \frac{(2\mu + k)a^2}{2r^3} \left[(B_2 - A_2) + \frac{3(B_2 - A_2) (1 - \alpha) \varepsilon (1 + \delta a)}{\Lambda_2} \right] (3 \cos^2 \theta - 1) + p_\infty, \end{aligned} \quad (3.76)$$

where p_∞ (arbitrary integration constant) is added for the constant pressure.

Now the radial component of the stress tensor for the micropolar fluid is obtained from (2.1) as follows.

$$T_{rr}^{2M} = p^{2M} - \bar{T}_{rr}^{2M}, \quad (3.77)$$

where

$$\bar{T}_{rr}^{2M} = (2\mu + k) \frac{\partial u_r^{2M}}{\partial r}. \quad (3.78)$$

Using the equation (3.72) in (3.77) and (3.78) we get

$$\begin{aligned}
(2\mu + k) \frac{\partial u_r^{2M}}{\partial r} &= (2\mu + k) \left[\bar{U} (1 + \Gamma_1) \left(\frac{3a^3}{r^4} - \frac{a}{r^2} \right) - 3(U + A_1) \left(\frac{a^3}{r^4} \right) \right. \\
&+ 2\bar{U}\Gamma_1 \left(\frac{3a^3}{r^3} \left(\frac{1}{\delta a} + \frac{1}{\delta^2 a^2} \right) - \frac{3ae^{\delta(a-r)}}{r} \left(\frac{1}{\delta r} + \frac{1}{\delta^2 r^2} \right) - \frac{ae^{\delta(a-r)}}{r^2} \right) \left. \right] \cos \theta \\
&- (2\mu + k) \left[B_2 \left(\frac{2a^4}{r^5} - \frac{a^2}{r^3} \right) + A_2 \left(\frac{a^2}{r^3} \right) \right. \\
&- 3(B_2 - A_2)\Gamma_2 \left\{ \left(2 \left(\frac{a^4}{r^5} \right) (1 + \delta a) - \left(\frac{a^2}{r^3} \right) (1 + \delta a) - \left(\frac{a^2 e^{\delta(a-r)}}{r^3} \right) (1 + \delta r) \right) \right. \\
&+ 4 \left. \left. \left(\left(\frac{a^4}{r^5} \right) \left(1 + \frac{3}{\delta a} + \frac{3}{\delta^2 a^2} \right) - \left(\frac{a^2 e^{\delta(a-r)}}{r^3} \right) \left(1 + \frac{3}{\delta r} + \frac{3}{\delta^2 r^2} \right) \right) \right\} \right] (3 \cos^2 \theta - 1), \quad (3.79)
\end{aligned}$$

where for convenience we have defined

$$\bar{U} = \frac{(3U - 2B_1 + A_1)}{2}, \quad \Gamma_1 = \frac{(1 - \alpha)\varepsilon}{\Lambda_1}, \quad \Gamma_2 = \frac{(1 - \alpha)\varepsilon}{\Lambda_2}.$$

Note that on the surface of the squirmer ($r = a$), the radial component of stress simplifies to

$$\boxed{T_{rr}^{2M}(a, \theta) = \frac{(2\mu + k)}{a} \left[\left\{ \frac{D_1}{a} + 2(A_1 + B_1) \right\} \cos \theta + \left\{ \frac{3D_2}{a^2} + A_2 + B_2 \right\} (3 \cos^2 \theta - 1) \right] - p_\infty.} \quad (3.80)$$

In a similar way the tangential stress component is determined using (2.1). We have

$$T_{r\theta}^{2M}(r, \theta) = -\mu \left(\frac{1}{r} \frac{\partial u_r^{2M}}{\partial \theta} - \frac{u_\theta^{2M}}{r} + \frac{\partial u_\theta^{2M}}{\partial r} \right) - k \left(\frac{\partial u_\theta^{2M}}{\partial r} - \Omega^{2M} \right), \quad (3.81)$$

Now, using (3.72)-(3.74) in (3.81) we get

$$\begin{aligned}
\mu \left(\frac{1}{r} \frac{\partial u_r^{2M}}{\partial \theta} - \frac{u_\theta^{2M}}{r} + \frac{\partial u_\theta^{2M}}{\partial r} \right) &= \mu \left[\bar{U} (1 + 3\Gamma_1) \left(\frac{a^3}{r^4} \right) - 2(A_1 + B_1) \left(\frac{a^3}{r^4} \right) - 2\bar{U}\Gamma_1 \left(\frac{ae^{\delta(a-r)}}{r^2} \right) \right. \\
&- 6\bar{U}\Gamma_1 \left(\frac{a}{r} \right) \left(\frac{a^2}{r^3} \left(\frac{1}{\delta a} + \frac{1}{\delta^2 a^2} \right) - e^{\delta(a-r)} \left(\frac{1}{\delta r} + \frac{1}{\delta^2 r^2} \right) \right) - \bar{U}\Gamma_1 (1 + \delta r) \left(\frac{ae^{\delta(a-r)}}{r^2} \right) \left. \right] \sin \theta \\
&- \mu \left[B_2 \left(\frac{8a^4}{r^5} - \frac{3a^2}{r^3} \right) + 3A_2 \left(\frac{a^2}{r^3} \right) \right. \\
&+ 3(B_2 - A_2)\Gamma_2 \left\{ \left(8(1 + \delta a) \left(\frac{a^4}{r^5} \right) - 3(1 + \delta a) \left(\frac{a^2}{r^3} \right) - 2 \left(\frac{a^2 e^{\delta(a-r)}}{r^3} \right) (1 + \delta r) \right) \right. \\
&+ 16 \left(\left(\frac{a^4}{r^5} \right) \left(1 + \frac{3}{\delta a} + \frac{3}{\delta^2 a^2} \right) - \left(\frac{a^2 e^{\delta(a-r)}}{r^3} \right) \left(1 + \frac{3}{\delta r} + \frac{3}{\delta^2 r^2} \right) \right) \\
&\left. \left. + \left(\frac{a^2}{r^3} \right) e^{\delta(a-r)} (\delta^2 r^2 + 3\delta r + 3) \right\} \right] \cos \theta \sin \theta, \tag{3.82}
\end{aligned}$$

$$\begin{aligned}
k \left(\frac{\partial u_\theta^{2M}}{\partial r} - \Omega^{2M} \right) &= k \left[\frac{\bar{U}}{2} (1 + 3\Gamma_1) \left(\frac{a^3}{r^4} \right) - (A_1 + B_1) \left(\frac{a^3}{r^4} \right) - \bar{U}\Gamma_1 \left(\frac{ae^{\delta(a-r)}}{r^2} \right) \right. \\
&- 3\bar{U}\Gamma_1 \left(\left(\frac{a^3}{r^4} \right) \left(\frac{1}{\delta a} + \frac{1}{\delta^2 a^2} \right) - e^{\delta(a-r)} \left(\frac{1}{\delta r} + \frac{1}{\delta^2 r^2} \right) \right) + \bar{U}\Gamma_1 \left(\frac{ae^{\delta(a-r)}}{r^2} (1 + \delta r) \frac{\mu}{k} \right) \left. \right] \sin \theta \\
&- k \left[B_2 \left(\frac{4a^4}{r^5} - \frac{3a^2}{2r^3} \right) + \frac{3A_2}{2} \left(\frac{a^2}{r^3} \right) + 3(B_2 - A_2)\Gamma_2 \left\{ \frac{5(1 + \delta a)}{2} \left(\frac{a^2}{r^3} \right) - \left(\frac{a^2}{r^3} \right) e^{\delta(a-r)} (1 + \delta r) \right. \right. \\
&+ 8 \left(\left(\frac{a^4}{r^5} \right) \left(1 + \frac{3}{\delta a} + \frac{3}{\delta^2 a^2} \right) - \left(\frac{a^2}{r^3} \right) e^{\delta(a-r)} \left(1 + \frac{3}{\delta r} + \frac{3}{\delta^2 r^2} \right) \right) \\
&\left. \left. - \left(\frac{a^2}{r^3} \right) e^{\delta(a-r)} (\delta^2 r^2 + 3\delta r + 3) \left(\frac{\mu}{k} \right) \right\} \right] \cos \theta \sin \theta, \tag{3.83}
\end{aligned}$$

\bar{U} , Γ_1 , and Γ_2 are defined just after equation (3.79). The above expression for the tangential stress component on the spherical squirmer $r = a$ reduces to

$$\boxed{T_{r\theta}^{2M}(a, \theta) = \frac{(2\mu + k)}{a} \left[\left\{ -\frac{D_1}{a} + (A_1 + B_1) \right\} \sin \theta + \left\{ -\frac{9D_2}{a^2} + (3A_2 + B_2) \right\} \cos \theta \sin \theta \right]}. \tag{3.84}$$

3.2 Swimming Speed, Power and Efficiency Calculations from the 2-Mode Solutions

Theoretical results for the speed, power, and efficiency can be very useful to understand the swimming characteristics. Here we provide the derivation of these important quantities for a spherical swimmer in the micropolar fluid using the 2-Mode solutions. In order to determine the swimming velocity (speed), one needs to find the force on the squirmer translating in micropolar fluid and then use the force-free condition [2, 17] to find the speed. To this end, we follow the procedure used in [12] for the calculation of the drag/force on the rigid sphere. The formula for the drag is [12]

$$F_r = \oint (T_{rr}^{2M} \cos \theta - T_{r\theta}^{2M} \sin \theta)_{r=a} d\theta, \quad (3.85)$$

where

$$\begin{aligned} (T_{rr}^{2M} \cos \theta)_{r=a} &= \frac{(2\mu + k)}{a} \left[\left\{ \frac{(3U - 2B_1 + A_1)}{4} (1 + \Gamma_1) + 2(A_1 + B_1) \right\} \cos^2 \theta \right. \\ &\quad \left. + \left\{ -\frac{(B_2 - A_2)}{2} (1 + 3\Gamma_2 (1 + \delta a)) + A_2 + B_2 \right\} (3 \cos^2 \theta - 1) \cos \theta \right] \end{aligned} \quad (3.86)$$

$$\begin{aligned} (T_{r\theta}^{2M} \cos \theta)_{r=a} &= \frac{(2\mu + k)}{a} \left[\left\{ -\frac{(3U - 2B_1 + A_1)}{4} (1 + \Gamma_1) + (A_1 + B_1) \right\} \sin^2 \theta \right. \\ &\quad \left. + \left\{ \frac{3(B_2 - A_2)}{2} (1 + 3\Gamma_2 (1 + \delta a)) + 3A_2 + B_2 \right\} \cos \theta \sin^2 \theta \right]. \end{aligned} \quad (3.87)$$

Substituting (3.86) and (3.87) in (3.85) and evaluating the integral using the orthogonality properties (see *Appendix B*, (B-1),(B-2)), one arrives at

$$F_r = (3U - 2B_1 + A_1) \pi a (2\mu + k) (1 + \Gamma_1). \quad (3.88)$$

The expression for the force in (3.88) may be decomposed in the form,

$$F_r = D_p + D_f, \quad (3.89)$$

where

$$D_p = \frac{2}{3} \left(\frac{(3U - 2B_1 + A_1)(1 + \Gamma_1)}{4a} \right), \quad D_f = 2D_p. \quad (3.90)$$

In (3.90), D_p and D_f are the contributions due to the pressure and frictional parts to the total drag. If we set $A_1 = B_1 = 0$ in (3.90), we recover the result presented in [19]. Now using the force-free condition

$$F_r = 0, \quad (3.91)$$

we obtain the swimming speed for a spherical squirmer in micropolar fluid as,

$$\boxed{U = \frac{2B_1}{3} - \frac{A_1}{3}}. \quad (3.92)$$

It is interesting that the swimming speed is independent of the micropolar fluid parameters. We note that the swimming speed in (3.92) is exactly the same as that for a squirmer in Stokes flow obtained by Lighthill [15] and Blake [2]. This in turn implies that a spherical squirmer in micropolar fluid swims with the same speed as in Stokes flow.

The power P (or the net work rate) generated on the surface of the spherical squirmer for its locomotion can be calculated by mimicking the approach used for Stokes flow [2, 15]. As in Stokes case, the power is computed from

$$P^{2M} = (2\pi) \int_0^\pi ((u_r^{2M} T_{rr}^{2M} + u_\theta^{2M} T_{r\theta}^{2M})_{r=a}) (a^2 \sin \theta) d\theta. \quad (3.93)$$

Using (3.57)-(3.58) and (3.86)-(3.87) we get

$$\begin{aligned} (u_r^{2M} T_{rr}^{2M})_{r=a} &= \frac{(2\mu + k)}{a} \left[A_1 \cos \theta + \frac{A_2}{2} (3 \cos^2 \theta - 1) \right] \\ &\times \left[2(A_1 + B_1) \cos \theta + \left\{ \frac{3D_2}{a^2} + A_2 + B_2 \right\} (3 \cos^2 \theta - 1) \right], \end{aligned} \quad (3.94)$$

$$\begin{aligned} (u_\theta^{2M} T_{r\theta}^{2M})_{r=a} &= \frac{(2\mu + k)}{a} [B_1 \sin \theta + B_2 \sin \theta \cos \theta] \\ &\times \left[(A_1 + B_1) \sin \theta + \left\{ -\frac{9D_2}{a^2} + (3A_2 + B_2) \right\} \cos \theta \sin \theta \right]. \end{aligned} \quad (3.95)$$

Substitution of (3.94) and (3.95) on (3.93) results in the following expression for the squirmer power in micropolar fluid

$$\boxed{P^{2M} = 2\pi a(2\mu + k) \left[\frac{4}{3}(A_1 + B_1)^2 + \frac{12D_2(A_2 - B_2)}{5a^2} + \frac{4}{5} \left(A_2^2 + \frac{B_2^2}{3} + 2A_2 B_2 \right) \right]}. \quad (3.96)$$

Where D_2 is given in (3.71) in terms of ε , δ , and α . Note that the power depends on the micropolar fluid parameter via the second mode. In the limit $k \rightarrow 0$ (or equivalently, $(\varepsilon \rightarrow 0)$), the above equation (3.96) reduces to the power for the 2-Mode squirmer in Newtonian fluid [2] as shown below

$$P^{2M} = 2\pi\mu a \left[\frac{8A_1^2}{3} + \frac{8B_1^2}{3} + \frac{16A_1B_1}{3} + \left(\frac{12A_2^2}{5} + \frac{4B_2^2}{3} + \frac{8A_2B_2}{5} \right) \right].$$

The results for the power and the drag on an isolated sphere translating in a micropolar fluid are sufficient to compute the hydrodynamic efficiency. As in [2], the efficiency η is calculated from

$$\eta = \frac{F_r U}{P^{2M}}, \quad (3.97)$$

where F_r is the drag due to the translation of a sphere given by

$$F_r = 3\pi U a (2\mu + k) (1 + \Gamma_1). \quad (3.98)$$

The above expression is extracted from (3.88) with $A_1 = B_1 = 0$. Below we derive the hydrodynamic efficiency for tangential and radial modes separately from the 2-Mode solutions. When the radial mode is absent the swimming speed given in (3.92) becomes

$$U = \frac{2}{3} B_1. \quad (3.99)$$

Using (3.99) in (3.98) one obtains

$$F_r = 2\pi B_1 a (2\mu + k) (1 + \Gamma_1). \quad (3.100)$$

Now the 2-Mode expression for the power (equation (3.96)) in the absence of radial modes becomes

$$P^{2M} = 2\pi a (2\mu + k) \left[\frac{4B_1^2}{3} + \frac{6B_2^2 \Gamma_2 (1 + \delta a)}{5} + \frac{2B_2^2}{3} \right]. \quad (3.101)$$

Substituting (3.99) – (3.101) in (3.97) we get

$$\eta = \left(\frac{1 + \Gamma_1}{2 + \beta^2 + \frac{9\beta^2 \Gamma_2 (1 + \delta a)}{5}} \right). \quad (3.102)$$

where we have taken $\beta = \frac{B_2}{B_1}$. The limit $k \rightarrow 0$ yields

$$\boxed{\eta = \frac{1}{2 + \beta^2}}. \quad (3.103)$$

which corresponds stokes flow result as expected.

In the same way we can obtain the efficiency for the radial modes (without the tangential modes).

The swimming speed in this case is

$$U = -\frac{A_1}{3}, \quad (3.104)$$

and the drag force is

$$F_r = -\pi A_1 a (2\mu + k) (1 + \Gamma_1). \quad (3.105)$$

The 2-mode power expression with only radial modes is

$$P^{2M} = 2\pi a (2\mu + k) \left[\frac{4A_1^2}{3} + \frac{16A_2^2}{5} + \frac{16A_2^2}{5} \Gamma_2 (1 + \delta a) \right]. \quad (3.106)$$

And now the efficiency η is

$$\boxed{\eta = \frac{1 + \Gamma_1}{8 \left(1 + \frac{9\xi^2}{10} (1 + \Gamma_2 (1 + \delta a)) \right)}}. \quad (3.107)$$

where $\xi = \frac{A_2}{A_1}$, and in the limit $k \rightarrow 0$ the result reduces to

$$\boxed{\eta = \frac{1}{8 + \frac{36\xi^2}{5}}}. \quad (3.108)$$

as it should. As in the case of power, the efficiency also depends on the micropolar fluid parameter in the second mode. We will use the 2-Mode results in **Chapter 4** and interpret the squirmer characteristics and discuss some flow details.

3.3 n -Mode Results for a Squirmer in Micropolar Fluid

The general n -mode results for the squirmer problem in the micropolar fluid can be obtained using the same steps used in the previous section. The expressions for the velocity components, micro-rotation, pressure, stress components, and power for the general case are provided below.

The stream function for the n -mode problem is given in (2.54). From this equation and (2.55), the velocity and the micro-rotation are

$$u_r^{nM}(a, \theta) = -U \cos \theta + \left(\frac{2C_1}{r^3} + \frac{2D_1}{r} + \frac{2F_1}{\delta^2 r^{\frac{3}{2}}} K_{\frac{3}{2}}(\delta r) \right) \cos \theta + \sum_{n=2}^{\infty} (n(n+1)) \left[\frac{C_n}{r^{n+2}} + \frac{D_n}{r^n} + \frac{F_n}{\delta^2 r^{\frac{3}{2}}} K_{n+\frac{1}{2}}(\delta r) \right] P_n(\cos \theta), \quad (3.109)$$

$$u_{\theta}^{nM}(r, \theta) = U \sin \theta + \left(\frac{C_1}{r^3} - \frac{D_1}{r} + \frac{F_1}{\delta^2 r^{\frac{3}{2}}} (\delta r K_{\frac{1}{2}}(\delta r) + K_{\frac{3}{2}}(\delta r)) \right) \sin \theta - \sum_{n=2}^{\infty} \left[\frac{nC_n}{r^{n+2}} + \frac{(n-2)D_n}{r^n} + \frac{F_n}{\delta^2 r^{\frac{3}{2}}} (\delta r K_{n-\frac{1}{2}}(\delta r) + nK_{n+\frac{1}{2}}(\delta r)) \right] P_n^1(\cos \theta), \quad (3.110)$$

$$\Omega^{nM}(r, \theta) = \left(\frac{D_1}{r^2} - \left(\frac{1+\varepsilon}{2\varepsilon} \right) \frac{F_1}{\sqrt{r}} K_{\frac{3}{2}}(\delta r) \right) \sin \theta - \sum_{n=2}^{\infty} \left[\frac{(2n-1)D_n}{r^{n+1}} - \left(\frac{1+\varepsilon}{2\varepsilon} \right) \frac{F_n}{\sqrt{r}} K_{n+\frac{1}{2}}(\delta r) \right] P_n^1(\cos \theta), \quad (3.111)$$

where the constants for the first mode C_1 , F_1 , and D_1 are given in (3.64), (3.67) and (3.70) respectively. The constants C_n , F_n and D_n found using the boundary conditions (2.16) and (2.17) are given by

$$C_n = \frac{a^{n+2}}{2n(n+1)} [(2B_n - (n-2)A_n) + \frac{(2n-1)(1-\alpha)\varepsilon(2B_n - nA_n)}{\delta a \Lambda} (\delta a K_{n-\frac{1}{2}}(\delta a) + 2K_{n+\frac{1}{2}}(\delta a))], \quad (3.112)$$

$$F_n = -\frac{(2n-1)(1-\alpha)\varepsilon(2B_n - nA_n)\delta a^{\frac{1}{2}}}{n(n+1)\Lambda}, \quad (3.113)$$

$$D_n = -\frac{(2B_n - nA_n)a^n}{2n(n+1)} \left[1 + \frac{(2n-1)(1-\alpha)\varepsilon K_{n-\frac{1}{2}}(\delta a)}{\Lambda} \right], \quad (3.114)$$

where

$$\Lambda = (1 + \varepsilon(1 - \alpha)) \delta a K_{n+\frac{1}{2}}(\delta a) - (2n - 1)(1 - \alpha) \varepsilon K_{n-\frac{1}{2}}(\delta a).$$

The pressure field for the general n -mode case is

$$p^{nM}(r, \theta) = (2\mu + k) \sum_{n=1}^{\infty} \left[\frac{(2n-1)nD_n}{r^{n+1}} P_n(\cos \theta) \right] + p_{\infty}. \quad (3.115)$$

The radial component of stress is obtained using (3.77) and (3.78) as follows. We have

$$\begin{aligned}
\frac{\partial u_r^{nM}}{\partial r} = & \left[\bar{U} (1 + \Gamma_1) \left(\frac{3a^3}{r^4} - \frac{a}{r^2} \right) - 3(U + A_1) \left(\frac{a^3}{r^4} \right) \right. \\
& + 2\bar{U}\Gamma_1 \left(\frac{3a^3}{r^3} \left(\frac{1}{\delta a} + \frac{1}{\delta^2 a^2} \right) - \frac{3ae^{\delta(a-r)}}{r} \left(\frac{1}{\delta r} + \frac{1}{\delta^2 r^2} \right) - \frac{ae^{\delta(a-r)}}{r^2} \right) \left. \right] \cos \theta \\
& - \sum_{n=2}^{\infty} \left[B_n \left((n+2) \frac{a^{n+2}}{r^{n+3}} - n \frac{a^n}{r^{n+1}} \right) + A_n \left(\frac{n^2}{2} \frac{a^n}{r^{n+1}} - \frac{n^2-4}{2} \frac{a^{n+2}}{r^{n+3}} \right) \right. \\
& + \Gamma_n (2B_n - nA_n) \left(\frac{n+2}{2} \frac{a^{n+2}}{r^{n+3}} K_{n-\frac{1}{2}}(\delta a) - \frac{na^n}{2r^{n+1}} K_{n-\frac{1}{2}}(\delta a) - \frac{a^{\frac{1}{2}}}{r^{\frac{3}{2}}} K_{n-\frac{1}{2}}(\delta r) \right) \\
& \left. + \frac{\Gamma_n (2B_n - nA_n)}{\delta a} \left(\frac{(n+2)a^{n+2}}{r^{n+3}} K_{n+\frac{1}{2}}(\delta a) - \frac{(n+2)a^{\frac{3}{2}}}{r^{\frac{5}{2}}} K_{n+\frac{1}{2}}(\delta r) \right) \right] P_n(\cos \theta), \quad (3.116)
\end{aligned}$$

where

$$\Gamma_n = \frac{(2n-1)(1-\alpha)\varepsilon}{\Lambda},$$

\bar{U} and γ_1 are defined after the equation (3.79). On the surface of the sphere ($r = a$), (3.116) becomes

$$\left(\frac{\partial u_r^{nM}}{\partial r} \right)_{r=a} = \left(\frac{2}{a} \right) \sum_{n=1}^{\infty} (A_n + B_n) P_n(\cos \theta). \quad (3.117)$$

Therefore, the radial stress component on the boundary takes the form

$$\boxed{(T_{rr}^{nM})_{r=a} = \frac{(2\mu + k)}{a} \sum_{n=1}^{\infty} \left[\frac{(2n-1)nD_n}{a^n} + 2(A_n + B_n) \right] P_n(\cos \theta) - p_{\infty}.} \quad (3.118)$$

The tangential stress component using (3.81) is calculated as

$$\begin{aligned}
\mu \left(\frac{1}{r} \frac{\partial u_r^{nM}}{\partial \theta} - \frac{u_{\theta}^{nM}}{r} + \frac{\partial u_{\theta}^{nM}}{\partial r} \right) = & \mu \left[\left\{ \bar{U} (1 + 3\Gamma_1) \left(\frac{a^3}{r^4} \right) - 2(A_1 + B_1) \left(\frac{a^3}{r^4} \right) - 2\bar{U}\Gamma_1 \left(\frac{ae^{\delta(a-r)}}{r^2} \right) \right. \right. \\
& - 6\bar{U}\Gamma_1 \left(\frac{a}{r} \right) \left\{ \frac{a^2}{r^3} \left(\frac{1}{\delta a} + \frac{1}{\delta^2 a^2} \right) - e^{\delta(a-r)} \left(\frac{1}{\delta r} + \frac{1}{\delta^2 r^2} \right) \right\} - \bar{U}\Gamma_1 (1 + \delta r) \left(\frac{ae^{\delta(a-r)}}{r^2} \right) \left. \right\} \sin \theta \\
& + \sum_{n=2}^{\infty} \left[B_n \left\{ \left(\frac{2(n+2)}{n+1} \right) \frac{a^{n+2}}{r^{n+3}} - \left(\frac{2(n^2-1)}{n(n+1)} \right) \frac{a^n}{r^{n+1}} \right\} + A_n \left\{ \left(\frac{n^2-1}{n+1} \right) \frac{a^n}{r^{n+1}} - \left(\frac{n^2-4}{n+1} \right) \frac{a^{n+2}}{r^{n+3}} \right\} \right. \\
& + \frac{(2B_n - nA_n)\Gamma_n}{n(n+1)} \left\{ n(n+2) \frac{a^{n+2}}{r^{n+3}} K_{n-\frac{1}{2}}(\delta a) - (n^2-1) \frac{a^n}{r^{n+1}} K_{n-\frac{1}{2}}(\delta a) - \frac{2a^{\frac{1}{2}}}{r^{\frac{3}{2}}} K_{n-\frac{1}{2}}(\delta r) \right\} \\
& \left. + \frac{2(2B_n - nA_n)(n+2)\Gamma_n}{(n+1)\delta a} \left\{ \frac{a^{n+2}}{r^{n+3}} K_{n+\frac{1}{2}}(\delta a) - \frac{a^{\frac{3}{2}}}{r^{\frac{5}{2}}} K_{n+\frac{1}{2}}(\delta r) \right\} + \frac{F_n}{\sqrt{r}} K_{n+\frac{1}{2}}(\delta r) \right] P_n^1(\cos \theta) \right], \quad (3.119)
\end{aligned}$$

$$\begin{aligned}
k \left(\frac{\partial u_{\theta}^{nM}}{\partial r} - \Omega \right) = k \left[\left\{ \frac{\bar{U}}{2} (1 + 3\Gamma_1) \left(\frac{a^3}{r^4} \right) - (A_1 + B_1) \left(\frac{a^3}{r^4} \right) - \bar{U}\Gamma_1 \left(\frac{ae^{\delta(a-r)}}{r^2} \right) \right. \right. \\
- 3\bar{U}\Gamma_1 \left\{ \left(\frac{a^3}{r^4} \right) \left(\frac{1}{\delta a} + \frac{1}{\delta^2 a^2} \right) - e^{\delta(a-r)} \left(\frac{1}{\delta r} + \frac{1}{\delta^2 r^2} \right) \right\} + \bar{U}\Gamma_1 \left\{ \frac{ae^{\delta(a-r)}}{r^2} (1 + \delta r) \frac{\mu}{k} \right\} \left. \right\} \sin \theta \\
+ \sum_{n=2}^{\infty} \left[B_n \left\{ \left(\frac{(n+2)}{n+1} \right) \frac{a^{n+2}}{r^{n+3}} - \left(\frac{(n^2-1)}{n(n+1)} \right) \frac{a^n}{r^{n+1}} \right\} + A_n \left\{ \left(\frac{n^2-1}{2(n+1)} \right) \frac{a^n}{r^{n+1}} - \left(\frac{n^2-4}{2(n+1)} \right) \frac{a^{n+2}}{r^{n+3}} \right\} \right. \\
+ \frac{(2B_n - nA_n)\Gamma_n}{2n(n+1)} \left\{ n(n+2) \frac{a^{n+2}}{r^{n+3}} K_{n-\frac{1}{2}}(\delta a) - (n^2-1) \frac{a^n}{r^{n+1}} K_{n-\frac{1}{2}}(\delta a) - \frac{2a^{\frac{1}{2}}}{r^{\frac{3}{2}}} K_{n-\frac{1}{2}}(\delta r) \right\} \\
+ \left. \frac{(2B_n - nA_n)(n+2)\Gamma_n}{(n+1)\delta a} \left\{ \frac{a^{n+2}}{r^{n+3}} K_{n+\frac{1}{2}}(\delta a) - \frac{a^{\frac{3}{2}}}{r^{\frac{5}{2}}} K_{n+\frac{1}{2}}(\delta r) \right\} - \frac{\mu}{k} \frac{F_n}{\sqrt{r}} K_{n+\frac{1}{2}}(\delta r) \right] P_n^1(\cos \theta) \left. \right]. \tag{3.120}
\end{aligned}$$

Now the tangential stress on the sphere is given by

$$\boxed{(T_{r\theta}^{nM})_{r=a} = -\frac{(2\mu + k)}{a} \sum_{n=1}^{\infty} \left[-\frac{(2n-1)D_n}{a^n} + \frac{2B_n + n(n+1)A_n}{n(n+1)} \right] P_n^1(\cos \theta)}. \tag{3.121}$$

The power for the n -mode case in micropolar fluid is computed using (3.93). The product of the velocity and stress components on the surface are given in the form

$$(u_r^{nM} T_{rr}^{nM})_{r=a} = (2\mu + k) \sum_{n=1}^{\infty} \left(\frac{(2n-1)nD_n A_n}{a^{n+1}} + \frac{2n(n+1)(A_n^2 + A_n B_n)}{an(n+1)} \right) (P_n(\cos \theta))^2, \tag{3.122}$$

$$(u_{\theta}^{nM} T_{r\theta}^{nM})_{r=a} = (2\mu + k) \sum_{n=1}^{\infty} \left(-\frac{2(2n-1)D_n B_n}{n(n+1)a^{n+1}} + \frac{4B_n^2 + 2n(n+1)A_n B_n}{an^2(n+1)^2} \right) (P_n^1(\cos \theta))^2. \tag{3.123}$$

Substituting (3.122) and (3.123) in (3.93) and integrating the results in the required expression for the power. The orthogonality relations for the associated Legendre functions (for the angular coordinate θ) (see *Appendix B, (B-4), (B-5)*) are used in the evaluation of the integral. The explicit form of the result is written as

$$P^{nM} = P_1^{nM} + P_2^{nM}, \tag{3.124}$$

where

$$\boxed{P_1^{nM} = (2\mu + k)\pi a \left[\frac{8}{3}(A_1 + B_1)^2 + \sum_{n=2}^{\infty} \left(\frac{(4n^2 + 6n + 8)A_n^2}{(n+1)(2n+1)} + \frac{8B_n^2}{n(n+1)} + \frac{24A_n B_n}{(n+1)(2n+1)} \right) \right]},$$

$$P_2^{nM} = (2\mu + k)\pi a \sum_{n=2}^{\infty} \left(\frac{2(2n-1)^2(1-\alpha)\epsilon k_{n-\frac{1}{2}}(\delta a)(2B_n - nA_n)^2}{n(n+1)(2n+1)\Lambda} \right),$$

We note that as $k \rightarrow 0$, the above result reduces to

$$P^{nM} = 2\pi a \left[\frac{8}{3}(A_1 + B_1)^2 + \sum_{n=2}^{\infty} \left(\frac{(4n^2 + 6n + 8)A_n}{(n+1)(2n+1)} + \frac{8B_n^2}{n(n+1)} + \frac{24A_n B_n}{(n+1)(2n+1)} \right) \right]. \quad (3.125)$$

Equation (3.125) agrees with that obtained in [2] for the spherical squirmer in Stokes flow with n -modes. The efficiency calculations can be performed for the general n -mode case, but, will not be discussed here further.

We conclude this chapter with the comment that the swimming speed is independent of the micropolar fluid parameters. But, for any given mode, the other quantities such as the stream function, velocity components, microrotation, pressure, stresses, power, and efficiency depend on k (or equivalently, ϵ), γ and α . The discussion of the swimming and flow characteristics in micropolar fluid with 2-mode results are presented in the next chapter.

CHAPTER IV: INTERPRETATIONS OF TWO-MODE RESULTS FOR A SPHERICAL SQUIRMER IN MICROPOLAR FLUID

The 2-mode results have been successfully utilized to understand the swimming characteristics in Stokes and Brinkman fluid environments [2, 17]. Here we discuss the flow details for the micropolar fluids using the 2-mode solutions derived in the previous chapter. As noted in section 3.1, the swimming speed in the micropolar fluid is the same as in Stokes flow and therefore, does not depend on the material constant k and the angular viscosity coefficients α_1 , β_1 , γ , and the micro-rotation α . Further, only the first mode in the surface velocity contributes to the speed of the spherical squirmer in a micropolar fluid. The effects of all the parameters for a micropolar fluid can be seen starting from 2-Mode solutions. Below we demonstrate the dependence of the parameters α and $\varepsilon = k/(2\mu + k)$ in 2-Mode results graphically. The flow fields for 2-Mode solutions are also discussed using the corresponding expression for the stream function. As will be seen, our numerical results and the flow patterns for the stream function indicate the dominance of Stokes flow model swimming characteristics for a spherical squirmer in a micropolar fluid. We point out that a similar analysis for the n -mode calculations can be carried out in a similar fashion (although it is not done here).

Below, we first recapture some of the features of the 1-Mode results and then proceed to the interpretation of the 2-Mode solutions.

4.1 Features of 1-Mode Results

As demonstrated in the section 3.1, the swimming speed of a spherical squirmer in a micropolar fluid is given by

$$U = \frac{2B_1}{3} - \frac{A_1}{3}.$$

We observe that the speed is the same as in Stokes flow [2, 15] and does not depend on the parameters k , α_1 , β_1 , γ , and α . This means that a spherical squirmer swims in micropolar fluids with the same velocity as in Stokes flow. Substitution of the swimming speed in 1-Mode solutions yields

the velocity and micro-rotation components, reduced from (3.60), (3.61) and (3.62), as

$$\begin{aligned}u_r(r, \theta) &= -U \cos \theta + \frac{2}{3} \left(\frac{a^3}{r^3} \right) (A_1 + B_1) \cos \theta, \\u_\theta(r, \theta) &= U \sin \theta + \frac{1}{3} \left(\frac{a^3}{r^3} \right) (A_1 + B_1) \sin \theta, \\\Omega(r, \theta) &= 0.\end{aligned}$$

The above velocity components are the same as those in Stokes flow presented in [15] and [2]. The pressure corresponding to the free swimming is zero and the stress components are

$$\begin{aligned}T_{rr}(a, \theta) &= 2 \frac{(2\mu + k)}{a} (A_1 + B_1) \cos \theta, \\T_{r\theta}(a, \theta) &= \frac{(2\mu + k)}{a} (A_1 + B_1) \sin \theta.\end{aligned}$$

The power for 1-Mode solution is

$$P = 2\pi(2\mu + k)a \left[\frac{4A_1^2}{3} + \frac{4B_1^2}{3} + \frac{8A_1B_1}{3} \right],$$

and as $k \rightarrow 0$, it reduces to the power in the Newtonian case [2]

$$P = 2\pi\mu a \left[\frac{8A_1^2}{3} + \frac{8B_1^2}{3} + \frac{16A_1B_1}{3} \right].$$

The above results reveal that the swimming characteristics for micropolar fluids are identical to those for Newtonian (Stokes) fluids.

4.2 Power and Efficiency for Two-Mode Results

The expression for radial and tangential 2-Mode power is given in (3.96). In equations (3.107) and (3.102) the efficiency expressions for the 2-Mode oscillations with radial and tangential modes are provided separately. There are several constants in the swimming problem but we analyze the effects of the material constant ε and the micro-rotation parameter α fixing the values of the rest of the parameters. Interpretations by varying other parameters can be carried out in a similar fashion. One can see from these results that both power and efficiency depend on ε and α due to the inclusion of the second mode. Below we give the graphical representation of these results. Note that $\varepsilon = \frac{v_r}{v}$. We fix $v = 2.9 \times 10^{-3}$ as in [12] and chose different v_r to account for ε variation in our graphical illustrations. Also, we have chosen $\gamma = 10^{-6}$ as in [12].

Variation of Power with Micro-Rotation Parameter α

The variation of the power with the micro-rotation parameter is shown in Figure 4.6 for various values of ε . The plots indicate that the power variations for radial modes Figure 4.6 (a), tangential modes Figure 4.6 (b) and the combined radial and tangential modes Figure 4.6 (c) are qualitatively similar. Quantitative variations are apparent from these figures. The general trend is that the power increases with ν_r (or equivalently with ε) and decreases with the micro-rotation α . It is noted that for $\alpha = 1$ the numerical value of the power for the micropolar fluid approaches that of Newtonian fluid in all cases. It is also seen that the magnitude of the power with radial modes Figure 4.6 (a) is higher compared to that of tangential 2-Modes Figure 4.6 (b). The tangential modes tend to decrease the power as shown in Figure 4.6 (b). Whereas, the magnitude of power with the combination of radial and tangential modes Figure 4.6 (c) is the highest among others.

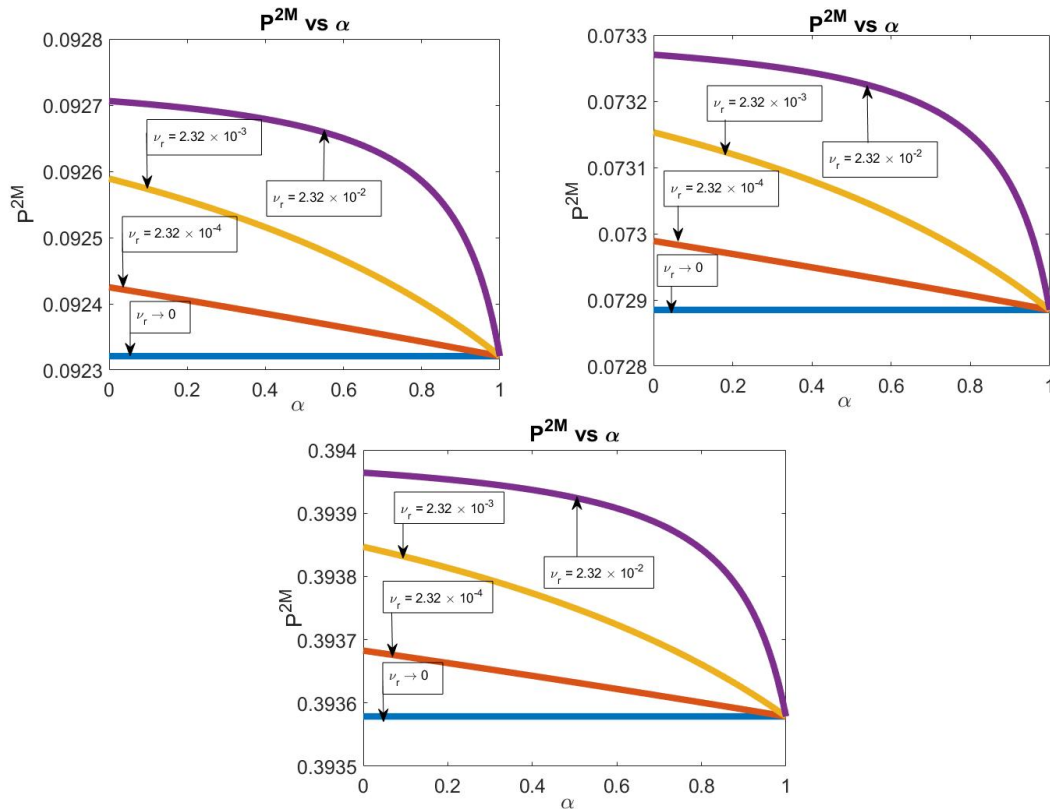


Figure 4.6
Variation of power vs α for (a) $A_2 = A_1 = 1$ and $B_1 = B_2 = 0$, (b) $A_2 = A_1 = 0$ and $B_1 = B_2 = 1$, (c) $A_2 = A_1 = 1$ and $B_1 = 1, B_2 = 2$

Variation of Power with Material Constant ϵ

The power variation with ϵ is displayed in Figure 4.7 for different values of α . It is seen that the power increases with the material constant ϵ in all cases. But it decreases with the micro-rotation parameter α . The power due to the combination of radial and tangential modes Figure 4.7 (c) is higher compared to that due to individual radial and tangential modes Figures 4.7 (a), (b).

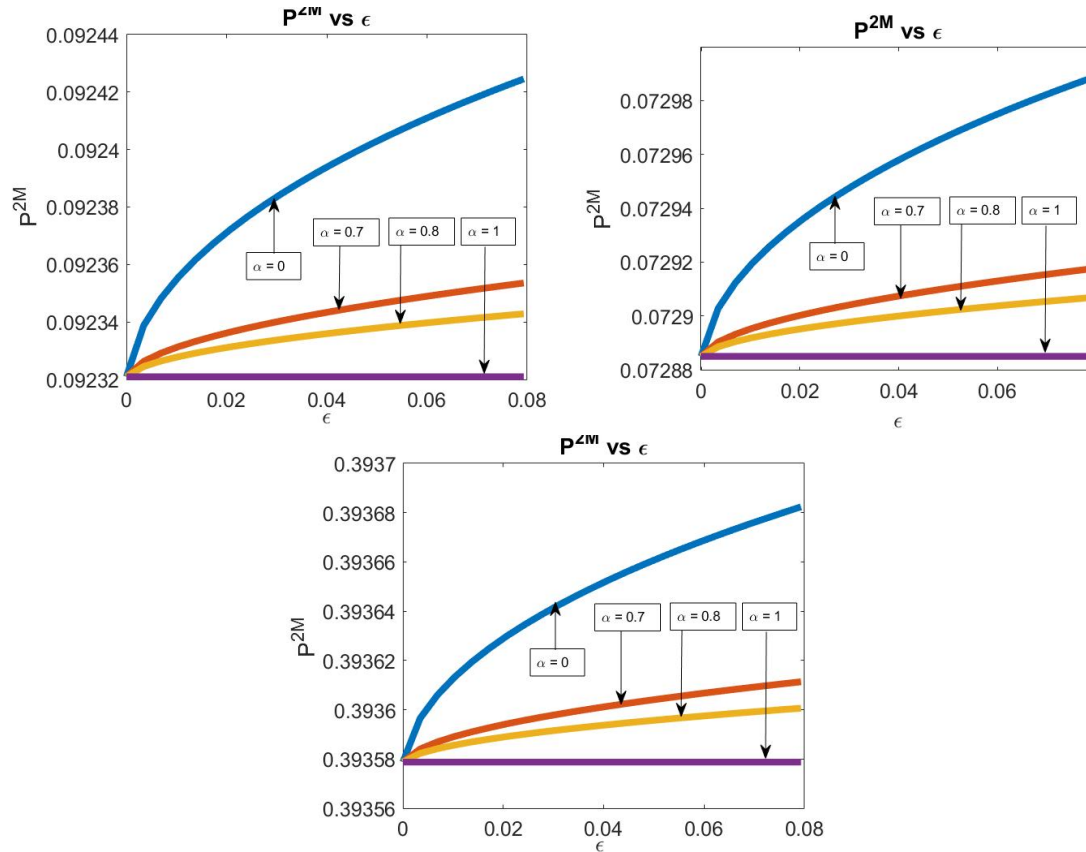


Figure 4.7

Variation of power vs ϵ for (a) $A_2 = A_1 = 1$ and $B_1 = B_2 = 0$ (b) $A_2 = A_1 = 0$ and $B_1 = B_2 = 1$ (c) $A_2 = A_1 = 1$ and $B_1 = 1, B_2 = 2$

Variation of Efficiency with Micro-Rotation Parameter α

The hydrodynamic efficiency η is plotted versus α using (3.107) and (3.102) and the representative plots are shown in Figure 4.8 (a) for the radial modes, in Figure 4.8 (b) for tangential modes, and in Figure 4.8 (c) for both together. It can be seen that the efficiency decreases with increasing α and approaches the Newtonian value as $\alpha \rightarrow 1$. Also, the plots show that the efficiency is greater than the corresponding Newtonian value in all cases considered here. This may indicate that the spherical squirmer can be efficient in micropolar fluid than in Stokes flow. Thus significant deviations can be observed in the micropolar fluid due to the presence of micro-rotation (and rotational viscosity ν_r).

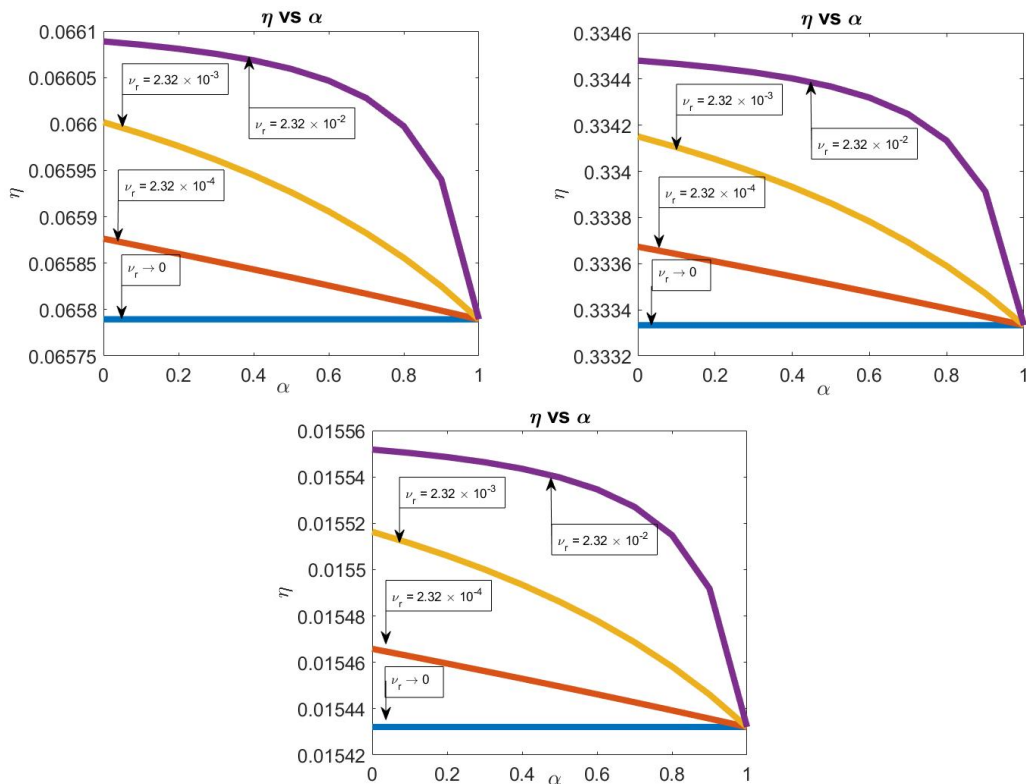


Figure 4.8
Variation of efficiency vs α for (a) $A_1 = A_2 = 1$ and $B_1 = B_2 = 0$ (b) $B_1 = B_2 = 1$ and $A_1 = A_2 = 0$ (c) $B_1 = 1$, $B_2 = 2$ and $A_1 = A_2 = 1$

Variation of η with Material Constant ε

The efficiency plots versus the material constant ε are displayed in Figure 4.9 (a), (b), (c) for radial, tangential, and sum of the two modes, respectively. The trend is similar to the variations

predicted for the power. The efficiency increases with increasing ϵ in all cases. The Newtonian efficiency can be recovered when $\alpha = 1$ (the bottom curve in all the cases shown here). This is the case when the micro-rotation completely vanishes on the boundary of the spherical squirmer. For $\alpha < 1$, the efficiency in the micropolar fluid is always greater than that in the Newtonian case. This is a different behavior compared to that observed in the Figure 4.8. Further, it appears that the efficiency can be made as large as we please for greater values of ϵ .

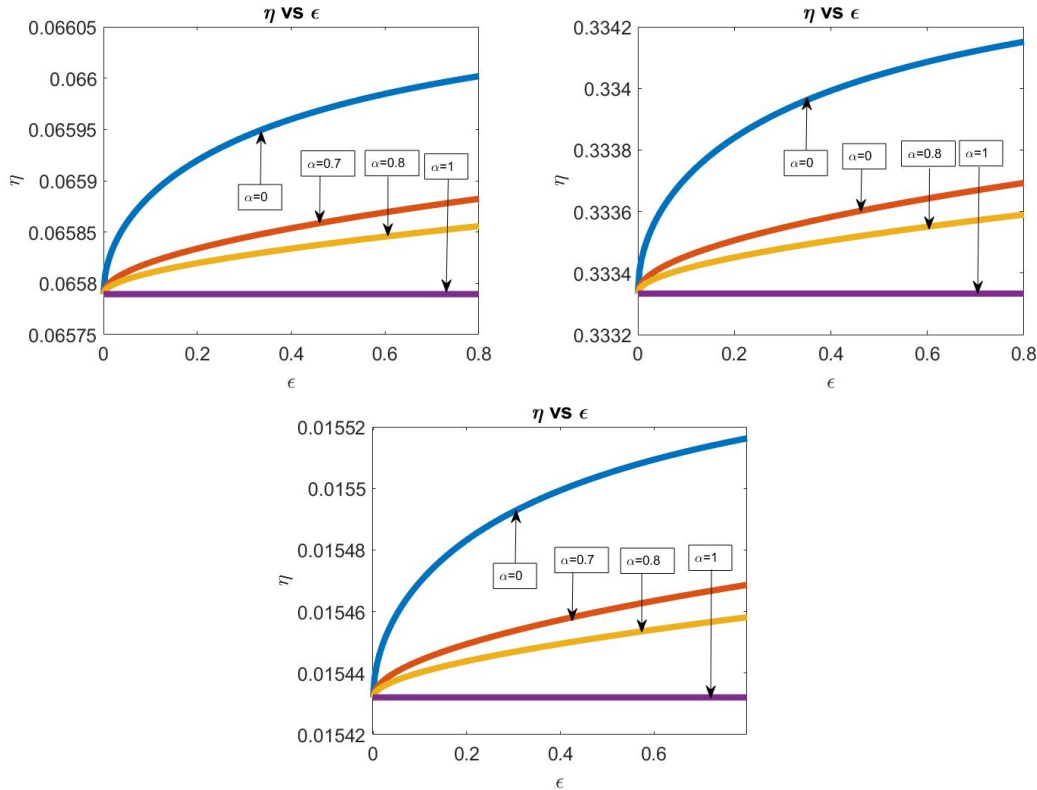


Figure 4.9
Variation of efficiency vs ϵ for (a) $A_1 = A_2 = 1$ and $B_1 = B_2 = 0$ (b) $B_1 = B_2 = 1$ and $A_1 = A_2 = 0$,
(c) $B_1 = 1$ $B_2 = 2$ and $A_1 = A_2 = 1$

4.3 Stokes Flow Dominance and Some Streamline Patterns

One of the surprising results found in the section 3.1 is that the swimming speed in micropolar fluid is the same as that in Stokes flow. Even though the micropolar fluid parameters appear in the stream function which provides a basic platform for all calculations, the speed is independent of these parameters. The cause for this may be understood by analyzing the stream function deeper.

To this end, we take the stream function solution for the second mode and write in the form

$$\psi(r, \theta) = \psi_S + \psi_B, \quad (4.126)$$

where

$$\begin{aligned} \psi_S &= \left[\frac{B_2}{2} \left(a^2 - \frac{a^4}{r^2} \right) - \frac{A_2 a^2}{2} + \frac{3(B_2 - A_2)\varepsilon(1 - \alpha)(1 + \delta a)}{2\Lambda_2} \left(a^2 - \frac{a^4}{r^2} \right) \right] \sin^2 \theta \cos \theta, \\ \psi_B &= \frac{3(B_2 - A_2)\varepsilon(1 - \alpha)}{\Lambda_2} \left[a^2 e^{\delta(a-r)} \left(1 + \frac{3}{\delta r} + \frac{3}{\delta^2 r^2} \right) - \frac{a^4}{r^2} \left(1 + \frac{3}{\delta a} + \frac{3}{\delta^2 a^2} \right) \right] \sin^2 \theta \cos \theta. \end{aligned}$$

We point out that the decomposition given in (4.126) is rather new and does not seem to have been reported earlier. The first term corresponds to the Stokes flow contribution and the second term is due to the Brinkman flow. Note that the magnitudes of these contributions are different from the classical Stokes and Brinkman flow fields, but depend on the micropolar fluid parameters. The numerical values of various contributions are tabulated in Tables 4.1 and 4.2 for certain fixed parameters. The corresponding stream functions values in the first and second quadrants when the x -coordinate of the point in the fluid domain is chosen closer the spherical squirmer is given in Table 4.1. The values for farther x -coordinate locations in the two quadrants are listed in Table 4.2. Comparison of Ψ_s (Column 5) with the total Ψ (Column 7) values reveal the dominance of Stokes flow. We observe that the Brinkman contribution (Column 6) is infinitesimally small to the micropolar fluid flow around the squirmer. Thus, one can say that the Stokes flow contribution dominates in the fluid domain when a spherical squirmer swims in micropolar fluids.

To illustrate this further we have plotted the flow streamlines corresponding to the second mode solution (4.126) in Figure 4.10 for some fixed values of the parameters. Stokes flow part is plotted in Figure 4.10 (a), Brinkman flow in Figure 4.10 (b) and the (total) micropolar fluid flow around the squirmer is shown in Figure 4.10 (c). It is clear from the plots that the streamlines are very similar to that in Stokes flow. While the Brinkman part shows a different pattern [17], the dominance of Stokes flow suppresses its contribution as shown in Figure 4.10 (c). The streamline plots shown here further supports our argument discussed in the preceding paragraph.

The flow is symmetric in all cases for the second mode as in Figure 4.10. The direction of the flow is also represented in the figure.

$\alpha = 0.5, v_r = 2.32 \times 10^{-4}, v = 2.9 \times 10^{-3}, \gamma = 10^{-6}$						
1ST QUADRANT						
X	Y	r	θ	ψ_S	ψ_B	ψ
1.2	0.6	1.3416	0.4636	0.0428	-2.49×10^{-04}	0.0425
1.2	1	1.5628	0.6947	0.0996	-3.23×10^{-04}	0.0994
1.2	1.4	1.8439	0.8622	0.1424	-2.76×10^{-04}	0.1421
1.2	1.8	2.1633	0.9828	0.1624	-2.05×10^{-04}	0.1622
1.2	2.2	2.506	1.0714	0.1669	-1.47×10^{-04}	0.1667
2nd QUADRANT						
X	Y	r	θ	ψ_S	ψ_B	ψ
-1.2	0.6	1.3416	2.6779	-0.0428	2.49×10^{-04}	-0.0425
-1.2	1	1.5628	2.4469	-0.0996	3.23×10^{-04}	-0.0994
-1.2	1.4	1.8439	2.2794	-0.1424	2.76×10^{-04}	-0.1421
-1.2	1.8	2.1633	2.1588	-0.1624	2.05×10^{-04}	-0.1622
-1.2	2.2	2.506	2.0701	-0.1669	1.47×10^{-04}	-0.1667

Table 4.1

Stream function values for closer x -coordinate values of a point in the fluid domain

$\alpha = 0.5, v_r = 2.32 \times 10^{-4}, v = 2.9 \times 10^{-3}, \gamma = 10^{-6}$						
1ST QUADRANT						
X	Y	r	θ	ψ_S	ψ_B	ψ
2.4	0.6	2.4739	0.245	0.0257	-2.33×10^{-5}	0.0257
2.4	1	2.6	0.3948	0.0626	-5.06×10^{-5}	0.0625
2.4	1.4	2.7785	0.5281	0.1027	-7.11×10^{-5}	0.1026
2.4	1.8	3	0.6435	0.1377	-8.01×10^{-5}	0.1376
2.4	2.2	3.2558	0.7419	0.1639	-7.95×10^{-5}	0.1639
2nd QUADRANT						
X	Y	r	θ	ψ_S	ψ_B	ψ
-2.4	0.6	2.4739	2.8966	-0.0257	2.33×10^{-5}	-0.0257
-2.4	1	2.6	2.7468	-0.0626	5.06×10^{-5}	-0.0625
-2.4	1.4	2.7785	2.6135	-0.1027	7.11×10^{-5}	-0.1026
-2.4	1.8	3	2.4981	-0.1377	8.01×10^{-5}	-0.1376
-2.4	2.2	3.2558	2.3996	-0.1639	7.95×10^{-5}	-0.1639

Table 4.2

Stream function values for farther x -coordinate values of a point in the fluid domain

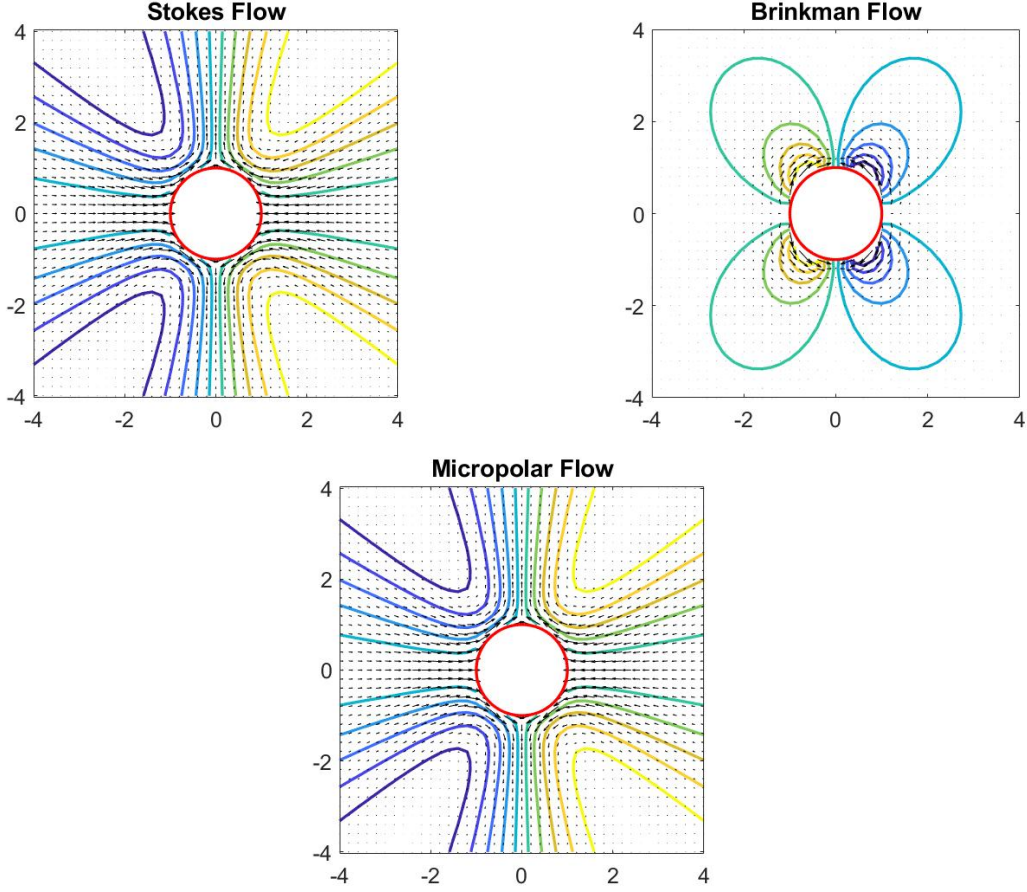


Figure 4.10

Streamline plots for $\alpha = 0.5$, $v = 2.9 \times 10^{-4}$, $v_r = 2.32 \times 10^{-3}$, $\gamma = 10^{-6}$ (a) Stokes Flow (b) Brinkman Flow (c) Micropolar Flow

4.4 Flow structure for Two-Mode Spherical Squirmer in Micropolar Fluids

The stream function for the two-mode self-propelling spherical squirmer (extracted from (equation 3.1) after substituting $U = \frac{2B_1}{3} - \frac{A_1}{3}$ along with $A_1 = 0$) is written as

$$\begin{aligned} \psi(r, \theta) = B_1 \left[\left(\frac{\beta}{2} \left(1 + \frac{\Gamma(1 + \delta a)}{2} \right) \left(a^2 - \frac{a^4}{r^2} \right) + \beta \Gamma \left(e^{\delta(a-r)} \left(1 + \frac{3}{\delta r} + \frac{3}{\delta^2 r^2} \right) \right. \right. \right. \\ \left. \left. - \left(\frac{a^2}{r^2} \right) \left(1 + \frac{3}{\delta a} + \frac{3}{\delta^2 a^2} \right) \right) \sin^2(\theta) \cos(\theta) - \left(\frac{a^3}{3r} \right) \sin^2(\theta) \right]. \end{aligned} \quad (4.127)$$

where $\beta = \frac{B_2}{B_1}$, $\Gamma = \frac{3B_2(1-\alpha)\varepsilon}{\Lambda_2}$ and Λ_2 is defined in the section 3.1. We have considered the tangential modes here and the radial mode analysis can be performed likewise. The self-propelled swimmer can be classified as a pusher $\beta = -1$, a neutral squirmer $\beta = 0$ and puller $\beta = 1$, and as in [17]. The streamline patterns for these classes of squirmers in micropolar fluid are depicted in Figure

4.11 (a), (b), (c), respectively. The flow patterns are very similar to the Stokes type flows [17]. This again supports the conclusion that the Stokes flow is dominant for a squirmer in micropolar fluid.

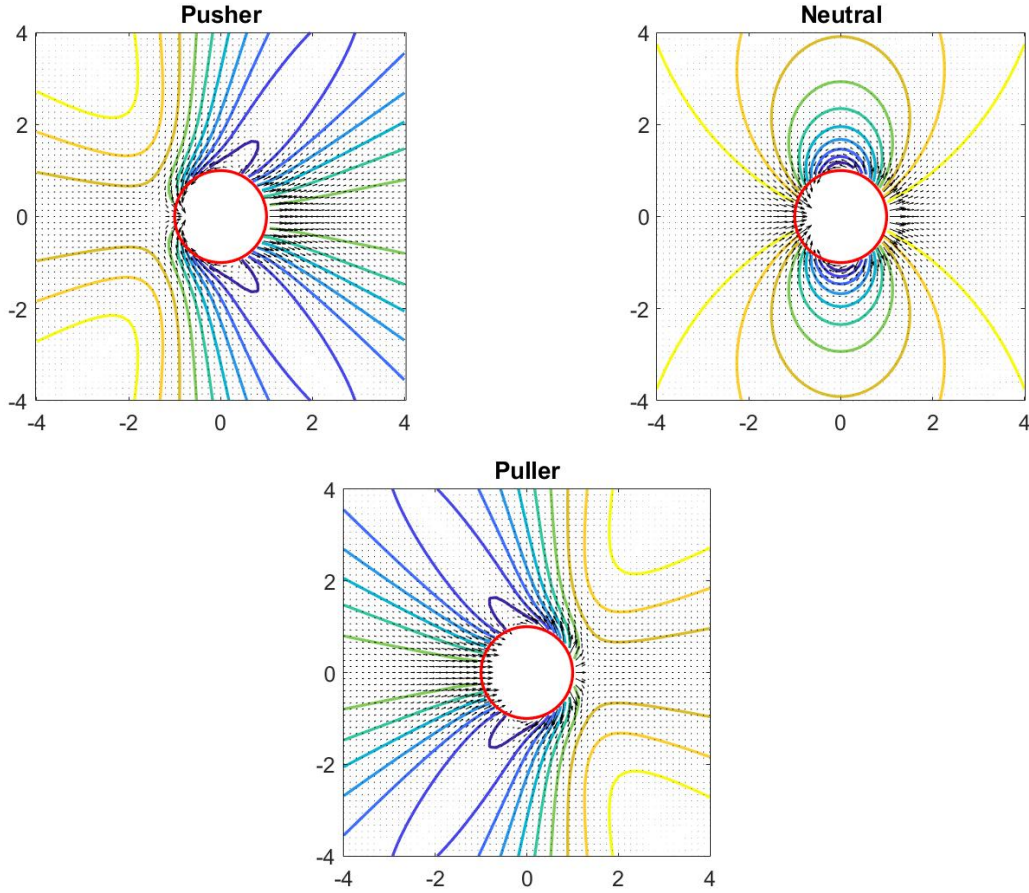


Figure 4.11
Swimming motion of the squirmer $\alpha = 0.5$, $v = 2.9 \times 10^{-4}$, $v_r = 2.32 \times 10^{-3}$, $\gamma = 10^{-6}$ (a) Pusher (b) Neutral (c) Puller

The micro-rotation equation for 2-mode free squirmer (extracted from equation (3.62)) is

$$\Omega(r, \theta) = -\frac{3(B_2 - A_2)}{2} \left(1 + \frac{3(1 - \alpha)\varepsilon(1 + \delta a)}{\Lambda_2} \right) \left(\frac{a^2}{r^3} \right) \sin \theta \cos \theta + \frac{3(B_2 - A_2)(1 - \alpha)\varepsilon}{\Lambda_2} \left(\frac{1 + \varepsilon}{2\varepsilon} \right) \left(\frac{a^2}{r^3} e^{\delta(a-r)} (\delta^2 r^2 + 3\delta r + 3) \right) \sin \theta \cos \theta. \quad (4.128)$$

Figure 4.12 illustrates the effect of micro-rotation due to the spherical squirmer in micropolar fluid for various values of the rotational viscosity v_r with $\alpha = 0.5$. Both radial and tangential modes are considered in this case. The micro-rotation contour plots shown in Figure 4.12 (a), (b), (c) indicate that the contour lines remain similar for different v_r values. There is a quadrupolar

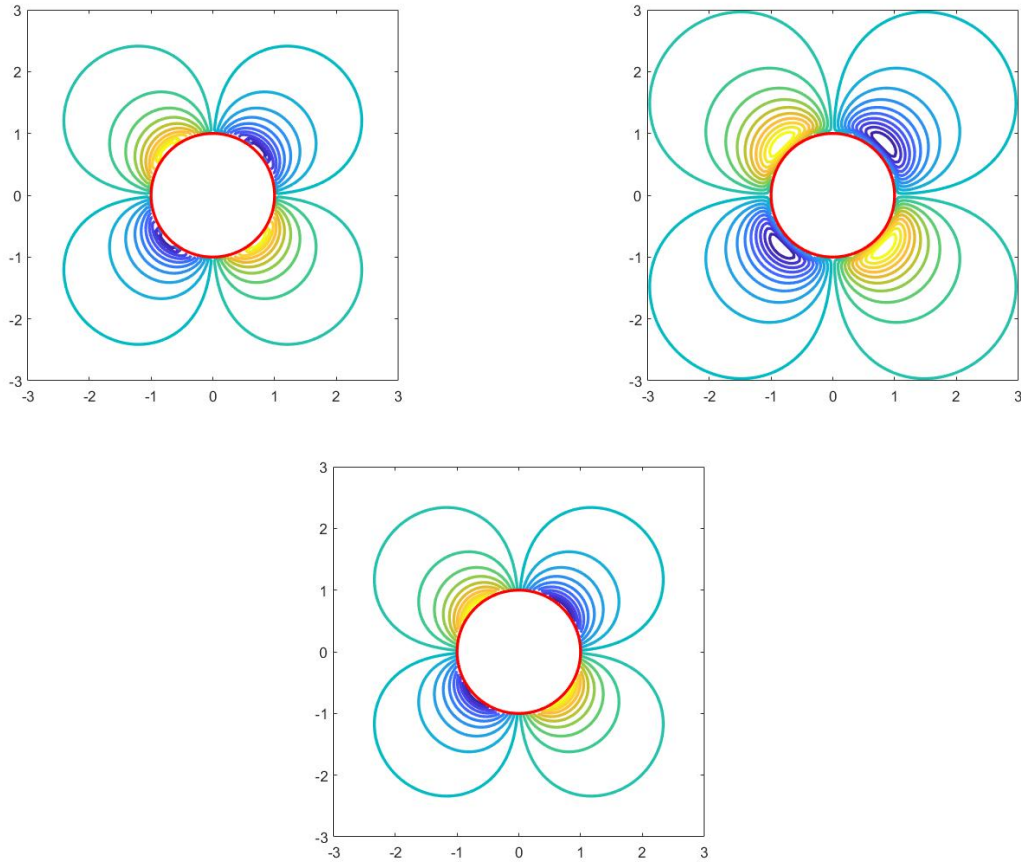


Figure 4.12

Micro-rotation distribution around the surface of the squirmer for $\alpha = 0.5$, $\nu = 2.9 \times 10^{-4}$, $\gamma = 10^{-6}$ (a) $\nu_r = 2.32 \times 10^0$ (b) $\nu_r = 2.32 \times 10^{-5}$ (c) $\nu_r = 2.32 \times 10^{-10}$

structure in all cases with a slight distributional change (not shown here) observed in the patterns values. Effects of the other micropolar fluid parameters can be analyzed in an analogous manner, but we will not present those results here.

CHAPTER V: SUMMARY AND CONCLUSION

The mathematical problem modeling a spherical squirmer in a micropolar fluid is treated with non-uniform surface velocity boundary conditions. Closed form analytical solutions are obtained by solving the sixth-order boundary value problem (BVP) for the stream function describing axisymmetric flows. The exact solutions of the BVP are then used to obtain expressions for the velocity, micro-rotation, pressure and stress fields. The swimming speed is calculated using the force-free condition and the power is determined via integrating the product of velocity and stresses on the spherical boundary. Our theoretical results show that the swimming velocity (speed) is independent of the micropolar fluid parameters- a surprising and interesting result.

The following specific conclusions can be drawn from our mathematical calculations for the squirmering sphere in micropolar fluids based on our calculations in this thesis

- The stream function depends on all the micropolar fluid parameters modeling the axisymmetric flow around the spherical swimmer.
- The swimming speed for a spherical squirmer in micropolar fluids is the same as that in Newtonian fluids.
- The velocity, pressure, micro-rotation, stress components, power and efficiency depend on the material constants k , γ , ε and the rotational parameter α for the 2-Mode and n -mode cases.
- Both the power and efficiency can increase or decrease with respect to the material constant ε and the micro-rotational parameter α .
- The spherical squirmer in micropolar fluid can be efficient than in Newtonian fluid for certain values of the parameters ε and α .
- Our theoretical solutions exactly reproduce the corresponding Newtonian results in Stokes flow in the limit of vanishing k (one of the key parameter characterizing micropolar fluid).

- Overall, the swimming characteristics can be adjusted based on the practical values of the parameters associated with the micropolar fluid.

The theoretical results for a squirming problem presented in this thesis are compact and can be implemented in practice with ease. We believe that our results can be utilized for a better understanding of various swimming mechanisms in media that depart from the classical Newtonian fluid. The generalization of the present model to include non-spherical geometrical shapes of the microorganisms is possible with appropriate modifications. The analysis of such general models and mathematical formulations can be relatively more challenging and will be the topics for future research.

APPENDIX A: Recurrence Relation for the Modified Spherical Bessel Functions of the Third Kind

The recurrence relations are provided for the Modified Spherical Bessel Functions of the third kind of order n , where $n \in \mathbb{Z}$ as in [1]

$$K_{-n-\frac{1}{2}}(\delta) = K_{n+\frac{1}{2}}(\delta) \quad (\text{A-1})$$

$$K_{n+\frac{1}{2}}(\delta) = K_{n+\frac{5}{2}}(\delta) - \frac{2(n+\frac{3}{2})}{\delta} K_{n+\frac{3}{2}}(\delta) \quad (\text{A-2})$$

$$K_{n+\frac{1}{2}}(\delta) = K_{n-\frac{3}{2}}(\delta) + \frac{2(n-\frac{1}{2})}{\delta} K_{n-\frac{1}{2}}(\delta) \quad (\text{A-3})$$

$$K_{n+\frac{1}{2}}(\delta) = \frac{\delta}{2n+1} \left(K_{n+\frac{3}{2}}(\delta) - K_{n-\frac{1}{2}}(\delta) \right) \quad (\text{A-4})$$

The following are the differentiation identities as given in [1]

$$\frac{dK_{n+\frac{1}{2}}(\delta)}{d\delta} = -\frac{1}{2} \left(K_{n+\frac{3}{2}}(\delta) + K_{n-\frac{1}{2}}(\delta) \right) \quad (\text{A-5})$$

$$\frac{dK_{n+\frac{1}{2}}(\delta)}{d\delta} = -K_{n-\frac{1}{2}}(\delta) - \frac{(n+\frac{1}{2})}{\delta} K_{n+\frac{1}{2}}(\delta) \quad (\text{A-6})$$

$$= \frac{(n+\frac{1}{2})}{\delta} K_{n+\frac{1}{2}}(\delta) - K_{n+\frac{3}{2}}(\delta) \quad (\text{A-7})$$

$$\frac{dK_0(\delta)}{d\delta} = -K_1(\delta) \quad (\text{A-8})$$

The Functions $K_{n+\frac{1}{2}}(\delta)$ for $n = 0, 1, 2$ referred from [1]

$$K_{m+\frac{1}{2}}(\delta) = K_{-m-\frac{1}{2}}(\delta) \quad (\text{A-9})$$

$$K_{\frac{1}{2}} = \sqrt{\frac{\pi}{2\delta}} e^{-\delta} \quad (\text{A-10})$$

$$K_{\frac{3}{2}} = \sqrt{\frac{\pi}{2\delta}} e^{-\delta} \left(1 + \frac{1}{\delta} \right) \quad (\text{A-11})$$

$$K_{\frac{5}{2}} = \sqrt{\frac{\pi}{2\delta}} e^{-\delta} \left(1 + \frac{3}{\delta} + \frac{3}{\delta^2} \right) \quad (\text{A-12})$$

APPENDIX B: Certain Properties of the Associated Legendre Functions

The following are orthogonal properties of the Associated Legendre functions in terms of polar angle θ over $[0, \pi]$ as in [1]

$$\int_0^\pi P_n^m(\cos \theta) P_l^m(\cos \theta) \sin \theta d\theta = 0 \quad (l \neq n) \quad (\text{B-1})$$

$$\int_0^\pi P_n^m(\cos \theta) P_n^l(\cos \theta) \csc \theta d\theta = 0 \quad (l \neq m) \quad (\text{B-2})$$

The following is the differentiation identity as in [1]

$$-\frac{1}{\sin \theta} \frac{d}{d\theta} (\sin \theta P_n^1(\cos \theta)) = n(n+1) P_n(\cos \theta) \quad (\text{B-3})$$

The following are the integral identities as in [1]

$$\int_0^\pi \sin \theta (P_n(\cos \theta))^2 d\theta = \frac{2}{2n+1} \quad (\text{B-4})$$

$$\int_0^\pi \sin \theta (P_n^1(\cos \theta))^2 d\theta = \frac{2n(n+1)}{2n+1} \quad (\text{B-5})$$

REFERENCES

- [1] Abramowitz, M., Stegun, I. A., and Romer, R. H. Handbook of mathematical functions with formulas, graphs, and mathematical tables, 1988.
- [2] Blake, J. R. A spherical envelope approach to ciliary propulsion. *Journal of Fluid Mechanics* 46, 1 (1971), 199–208.
- [3] Bray, D. *Cell movements: from molecules to motility*. 2000.
- [4] Brennen, C., and Winet, H. Fluid mechanics of propulsion by cilia and flagella. *Annual Review of Fluid Mechanics* 9, 1 (1977), 339–398.
- [5] Drescher, K., Leptos, K. C., Tuval, I., Ishikawa, T., Pedley, T. J., and Goldstein, R. E. Dancing volvox: hydrodynamic bound states of swimming algae. *Physical review letters* 102, 16 (2009), 168101.
- [6] Erdogan, M. E. Dynamics of polar fluids. *Acta Mechanica* 15, 3 (1972), 233–253.
- [7] Eringen, A. C. Simple microfluids. *International Journal of Engineering Science* 2, 2 (1964), 205–217.
- [8] Eringen, A. C. Theory of micropolar fluids. *Journal of Mathematics and Mechanics* (1966), 1–18.
- [9] Fauci, L. J., and Dillon, R. Biofluidmechanics of reproduction. *Annu. Rev. Fluid Mech.* 38 (2006), 371–394.
- [10] Hancock, G. The self-propulsion of microscopic organisms through liquids. *Proceedings of the Royal Society of London. Series A. Mathematical and Physical Sciences* 217, 1128 (1953), 96–121.
- [11] Happel, J., and Brenner, H. *Low Reynolds number hydrodynamics: with special applications to particulate media*, vol. 1, 2012.
- [12] Hoffmann, K.-H., Marx, D., and Botkin, N. D. Drag on spheres in micropolar fluids with non-zero boundary conditions for microrotations. *Journal of Fluid Mechanics* 590 (2007), 319–330.

- [13] Karvelas, E., Sofiadis, G., Papathanasiou, T., and Sarris, I. Effect of micropolar fluid properties on the blood flow in a human carotid model. *Fluids* 5, 3 (2020), 125.
- [14] Lauga, E., and Powers, T. R. The hydrodynamics of swimming microorganisms. *Reports on Progress in Physics* 72, 9 (2009), 096601.
- [15] Lighthill, M. On the squirming motion of nearly spherical deformable bodies through liquids at very small reynolds numbers. *Communications on pure and applied mathematics* 5, 2 (1952), 109–118.
- [16] Lukaszewicz, G. *Micropolar fluids: theory and applications*. 1999.
- [17] Nganguia, H., and Pak, O. S. Squirming motion in a brinkman medium. *Journal of Fluid Mechanics* 855 (2018), 554–573.
- [18] Rao, S. L., and Rao, P. B. The slow stationary flow of a micropolar liquid past a sphere. *Journal of Engineering Mathematics* 4, 3 (1970), 209–217.
- [19] Sawada, T., Kamata, T., Tanahashi, T., and Ando, T. Stokesian flow of a micropolar fluid past a sphere. *Keio Science and Technology Reports* 36, 4 (1983), 33–47.
- [20] Sleigh, M. Ciliary propulsion in protozoa. *Science Progress (1933-)* (1989), 317–331.
- [21] Tamm, S. L. Ciliary motion in paramecium: a scanning electron microscope study. *The journal of cell biology* 55, 1 (1972), 250–255.
- [22] Taylor, G. I. Analysis of the swimming of microscopic organisms. *Proceedings of the Royal Society of London. Series A. Mathematical and Physical Sciences* 209, 1099 (1951), 447–461.